Is Human Brain Activity During Driving Operations Modulated by the Viscoelastic Characteristics of a Steering Wheel?: An fMRI Study

YOSHIHISA OKAMOTO[1,2], (Member, IEEE), **TAKAFUMI SASAOKA**[3], **NORIHIRO SADATO**[4], **MASAKI FUKUNAGA**[4], **TETSUYA YAMAMOTO**[4], (Member, IEEE), **ZU SOH**[2], (Member, IEEE), **TAKAHIDE NOUZAWA**[5], **SHIGETO YAMAWAKI**[3], AND **TOSHIO TSUJI**[2], (Member, IEEE)

[1]Mazda Motor Corporation, Hiroshima 730-8670, Japan
[2]Department of System Cybernetics, Graduate School of Engineering, Hiroshima University, Hiroshima 739-8527, Japan
[3]Center for Brain, Mind and KANSEI Sciences Research, Hiroshima University, Hiroshima 734-8553, Japan
[4]Department of System Neuroscience, National Institute for Physiological Sciences, Okazaki 444-8585, Japan
[5]Office of Academic Research and Industry-Academia-Government and Community Collaboration, Hiroshima University, Hiroshima 739-8527, Japan

Corresponding authors: Yoshihisa Okamoto (okamoto_y@mazda.co.jp), Takafumi Sasaoka (tsasaoka@hiroshima-u.ac.jp), and Toshio Tsuji (tsuji@bsys.hiroshima-u.ac.jp)

ABSTRACT To date, a neuroscientific investigation of drivers' steering behavior has never been performed because the reaction forces generated by the mechanical characteristics of a steering wheel have been difficult to assess in a magnetic resonance imaging (MRI) environment. In this study, using our previously developed MRI-compatible unit for steering reaction force generation, we investigated changes in human brain activity induced by varying the viscoelastic characteristics associated with manipulating a car steering wheel. Participants performed a simulated driving task with three levels of stiffness and viscosity. An amplitude effect of reaction forces on the measured brain activity due to varying stiffness was found in the primary motor cortex (M1) associated with hand representation. Conversely, the changes in the brain activity induced by varying viscosity were found more dorsally in the premotor cortex and the M1 than in regions associated with hand representation. These results are the first to demonstrate that various viscoelastic characteristics activate different motor regions; more specifically, stiffness and viscosity of the steering wheel mainly affected the motor control of the distal and proximal muscles, respectively.

INDEX TERMS Brain activity, functional magnetic resonance imaging, steering reaction force, viscoelastic characteristics, proximal muscle, distal muscle.

I. INTRODUCTION

Electrically powered steering systems are commonly used, and steering reaction forces can be configured with high degrees of freedom as the result of progress in the research and development of electronic control technology (e.g., [1]). Therefore, it has been desirable to quantitatively optimize the characteristics of steering reaction forces. In order to efficiently configure mechanical steering characteristics, Takemura *et al.* [2] proposed a force perception model in

The associate editor coordinating the review of this manuscript and approving it for publication was Yi Zhang .

humans when performing steering operations; this model can be applied to configure the mechanical characteristics of the steering so that subjective perceptions of the steering reaction force change linearly in relation to the steering operation, facilitating better prediction of vehicle responses to steering.

Previous studies, however, have adopted an ergonomics-based approach to measuring behavioral and psychophysiological indices of the vehicle and driver, such as subjective evaluation of feelings experienced while driving, musculoskeletal activities related to steering behavior, and resultant emotional responses induced by the autonomic nervous system. Moreover, these measurements may further the

understanding of how steering reaction force characteristics affect the predictability of vehicular behavior, the operability of a vehicle, and the driving pleasure elicited by these factors (e.g., [3]–[5]). To date, unfortunately, the underlying mechanisms could only be indirectly estimated using these behavioral and psychophysiological indices.

On the other hand, researchers have recently proposed the use of ''neuroergonomic''-based approaches, combining neuroscientific findings and ergonomics [6]. It is possible that such approaches could reveal the neural basis of driving behavior, providing novel findings that could improve previous ergonomic theories and models that evaluated the relationships between a car and a driver [7], [8]. In particular, neuroimaging studies of car-driving using functional magnetic resonance imaging (fMRI) and driving simulators have been conducted since around the early 21st century. These previous studies revealed the neural substrates of driving under normal and disturbed conditions, including driving under the influence of alcohol (e.g., [6], [9]). It is possible that fMRI studies could better reveal the brain mechanisms associated with the ways that steering reaction force characteristics affect the vehicle's operability and the driver's perception, and may provide a stronger neuroscientific basis for the design of novel steering systems. Although several studies have performed fMRI experiments with steering wheels (e.g. [9], [10]), no fMRI study has examined the effect of the steering reaction forces fed back to the driver. To address this issue, we previously developed an fMRI-compatible steering reaction force generation unit [11]. To the best of our knowledge, this unit is the first equipment that enables performance of driving operations with reaction force feedback in an fMRI environment.

In the present study, we examined the neural basis of driving by measuring brain activity while performing a simulated driving task with different steering wheel viscoelastic characteristics (stiffness and viscosity of the steering reaction force) using the fMRI-compatible steering reaction force generation unit. Achieving a steering feeling within a range of small steering angles up to about 10 degrees is an important issue in vehicle development because this range is mainly used in daily driving; therefore, we focused on this range in our experiment. We used a simple linear relationship between steering angle and steering reaction force, whereas existing commercial vehicles have a comparatively more complex relationship. As the first step toward clarifying the neural basis for driving, we aimed to delineate the effects of stiffness and viscosity on driving behavior and brain activity by performing simple comparisons among conditions with different levels of stiffness and viscosity. Therefore, based on the linear approximation of the non-linear relationship between steering angle and reaction force used in existing commercial vehicles, we used a steering force that was characteristic of a linear relationship between the steering angle and the reaction force.

Stiffness and viscosity parameters of the steering wheel were varied to examine how viscoelastic parameters affect

motor control strategies. We investigated the neural basis of driving; in particular, motor planning and control associated with changing physical conditions and emotions related to driving pleasure. Changes in stiffness and viscosity characteristics of steering, which are mechanical, can be assumed to affect brain activity related to motor control. Furthermore, if the steering wheel characteristics impact the ease of driving, negative feelings should be elicited when a vehicle's response to the steering wheel input is not as expected, whereas positive feelings should be elicited when a vehicle response is as expected. Given that driving is considered a kind of goal-directed visuomotor behavior, drivers evaluate their task performance by monitoring prediction errors with respect to the vehicle's response. If a mechanical characteristic of the steering wheel is difficult to control, the driver's motivation may be affected and he or she may become irritated by being unable to reduce prediction error. In contrast, if a vehicle response is as expected, drivers can operate the vehicle without stress and can maintain their motivation, resulting in a positive feeling. Altogether, it can be expected that varying steering characteristics while driving should activate brain regions associated not only with motor control, but also with emotional processing caused by evaluation of prediction error in vehicular responses to steering operations.

II. METHODS
### A. APPARATUS
1) OVERALL STRUCTURE
Fig. 1 shows an experimental setting in which the steering reaction force can be manipulated in a simulated driving environment in an MRI scanner. The experimental system was configured using an fMRI-compatible steering reaction force generation unit [11], which we will refer to as ''the unit''. The unit consisted of a steering reaction force generation component and a reaction force transmission component, both of which made of non-magnetic materials. The unit generates force against the rotation and rotational velocity of the steering wheel according to preset mechanical characteristics. We improved the unit from the previous study [11] in three ways: (i) we increased the rigidity of the rotating shaft by improving the manufacturing method of the fiber reinforced plastic (FRP) material, (ii) we improved the stability of the shaft support component, and (iii) we replaced the motor with a specialized substitute that allowed for torque control.

2) PRESENTATION OF SIMULATED ROAD IMAGES
The driving simulator presented road images seen from a car traveling at a constant speed. Participants were allowed to operate the wheel to steer the car left and right in a supine posture, as shown in Fig.2. An MRI-compatible 32-inch liquid crystal display (LCD) monitor (NordicNeuroLab, Norway) with a resolution of $1,920 \times 1,080$ pixels was placed at the head side of the MRI scanner (left side of Fig. 1 (a)), upon which the simulated road images were presented with the left and right sides reversed. Participants could watch the
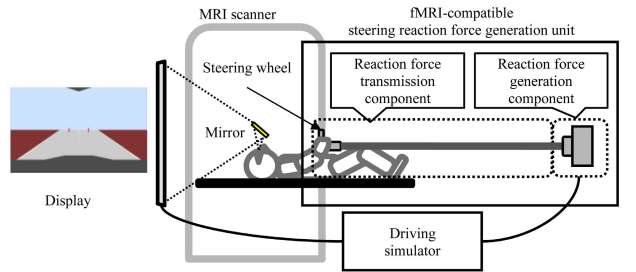
(a) Experimental system consisting of a functional magnetic resonance imaging (fMRI)-compatible steering reaction force generation and transmission unit.
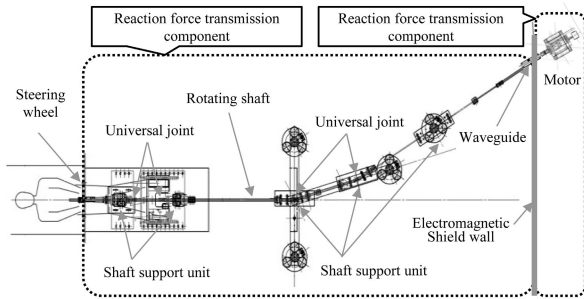
(b) Configuration of the fMRI-compatible steering reaction force generation system.

FIGURE 1. Experimental system for presenting steering reaction forces during simulated driving in a magnetic resonance imaging (MRI) scanner.

FIGURE 2. Steering posture with the participant in a supine position inside the gantry.

images through a mirror attached to the head coil. These configurations allowed participants to see the road images by naturally looking forward. In the experiment, we used a simple vehicle model because we needed our experimental design in a driving environment to be as simple as possible. In this model, a "camera" placed at the driver's point of view was set about 1300 mm above the road. When the vehicle moved, the camera position was translated forward at a constant speed, and the camera direction was rotated according to the yaw angle proportional to the steering angle. We used the OpenGL graphic library to render the camera view, which also included the road and the poles located on the road.

3) REACTION FORCE GENERATION

The reaction force was presented to participants according to the compliance control method given by (1). In this manuscript, we have used the terms stiffness and viscosity. In (1), stiffness refers to the element of the reaction force

generated in proportion to the magnitude of the rotation angle θ, which is generated by a steering operation. Viscosity is used as a term representing the element of the reaction force generated in proportion to θ velocity.

$$\frac{d^2\theta}{dt^2} = \frac{1}{J}\left(F - K_{stiff}\theta - \frac{d\theta}{dt}B_{visc}\right) \quad (1)$$

where

K_{stiff}: Stiffness coefficient, B_{visc}: Viscosity coefficient,
$\frac{d^2\theta}{dt^2}$: Angular acceleration = Motor control target value,
J: Inertia, and F: Measured torque

The reaction force generation component was installed outside the MRI scan room, separated by an electromagnetic shield, thereby preventing electromagnetic noise generated by the motor from affecting the MRI images (Fig.1 (b)). The rotating shaft of the reaction force generating motor was connected to the reaction force transmission component in the MRI scan room via a waveguide. To generate reaction force, we used a reaction force generation motor (Torque Actuator UNISERVO SVM-80 reduction rate 1/50 type, ROBOTEC Inc., Tokyo, Japan) and controller (SVC-80, ROBOTEC Inc. Tokyo, Japan). The torque-servo installed in this system allowed us to measure and control the torque at the output shaft.

B. EXPERIMENT

Two sets of experiments were performed to investigate the neurobehavioral effects of manipulating the steering reaction forces using three different levels of stiffness and viscosity parameters, represented by K_{stiff} and B_{visc} in (1), respectively. Hereafter, these sets of experiments will be referred to as the stiffness condition and the viscosity condition, respectively.

1) PARTICIPANTS

The participants consisted of 23 men (average age: 25.9 years (SD 5.2)) for the stiffness condition and 22 men (average age: 27.1 years (SD 5.2)) for the viscosity condition, none of whom had a history of neurological or psychiatric disorders. All participants were right-handed, as confirmed by the Edinburgh Handedness Inventory [12], had a driver's license and were driving on a daily basis.

These experiments were approved by the Research Ethics Committee of Hiroshima University and Mazda Motor Corporation (approval numbers E-965-5 and TRC-152-6). Prior to the experiment, we obtained written informed consent from all participants.

2) EXPERIMENTAL DESIGN

Table 1 shows the experimental parameters of the stiffness and viscosity conditions. K_{stiff} and B_{visc} in Table 1 are the stiffness coefficient and viscosity coefficient shown in (1). Each stiffness and viscosity coefficient conditions consisted of three levels. In the first level of the stiffness condition (S1), both coefficients were set to zero; in the first level of the viscosity conditions (V1), only the viscosity was set to zero. We considered S1 and V1 as the reference levels to examine

TABLE 1. Experimental condition: Motor control for reaction force generation.

	Stiffness condition			Viscosity condition		
	S1	S2	S3	V1	V2	V3
K_{stiff} (Nm/rad)	0.00	12.8	25.5	12.8		
B_{visc} (Nms/rad)	0.00			0.00	2.00	4.00
	$J = 0.02$ (Nms^2/rad)					

K_{stiff}: Stiffness coefficient, B_{visc}: Viscosity coefficient, J: Inertia

the effects of stiffness and viscosity. The second level of stiffness condition (S2) was then implemented by converting the steering angle-steering force characteristic into a simple linear relationship, based on the value of the steering angle-reaction force characteristic of existing commercial vehicles within a small steering angle range up to 10 degrees. In our preliminary pilot experiment outside the scanner, we confirmed that with the reaction force generated at this level, it was easy to steer in the supine posture, which was required for this experiment to be performed inside an MRI scanner. The third level of stiffness condition (S3) was the level at which the steering reaction force was felt to be slightly large in the supine position, which was achieved by setting the stiffness coefficient (K_{stiff}) in equation (1) to twice the value used for S2. We also confirmed that a large exertion force was not required for steering operations in the pilot experiment. For the three levels of the viscosity condition (V1-V3), the stiffness coefficients were the same as the second level of the stiffness condition (S2). In the first level of the viscosity condition (V1), the viscosity coefficient was set to zero; in the second level (V2), the viscosity coefficient was set to a value that gave a moderate response to participants, which made them feel the viscosity. The third level (V3) was the level that made participants feel a slightly excessive viscosity. The viscosity coefficient value used for V3 was twice of that for V2, and this viscosity was felt to be slightly high in the supine position, although we confirmed that participants could perform this task without much difficulty due to steering delay. Regarding the number of levels for each condition, we determined one condition with three levels that would fulfill the minimum requirement for our study aim, considering participants' fatigue.

The experimental protocol is shown in Fig. 3. The experiment consisted of six runs. The three levels of the parameters used for each condition are shown in Table 1 (K_{stiff}: S1, S2, S3 in the stiffness condition; B_{visc}: V1, V2, V3 in the viscosity condition). Each of the three levels of the parameters was randomly assigned to six runs, but we avoided assigning the same level to successive runs by assigning it only to the first or latter three runs.

As shown in Fig. 3, each run consists of practice and task phases. In the practice phase, participants practiced driving tasks and subjective evaluation using the visual analog
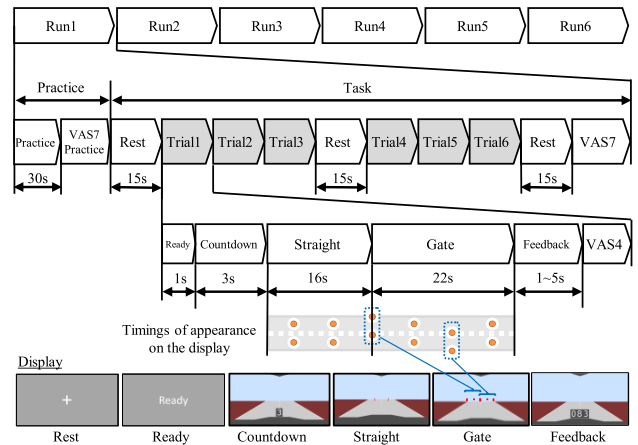

FIGURE 3. Schematic of the experimental protocol showing the timing and duration of each phase. VAS = visual analog scale.

TABLE 2. Words for subjective evaluation.

	Stiffness condition	Viscosity condition
VAS4	Self-efficacy Pleasantness Nimbleness Smoothness	Self-efficacy Pleasantness Nimbleness Smoothness
VAS7	Unpleasantness Self-efficacy Pleasantness Arousal Expectation Excitement Anxiety	Unpleasantness Self-efficacy Pleasantness Arousal Expectation Excitement Motivation

VAS = visual analog scale.

scale (VAS). In the task phase, participants performed six trials. After each trial, participants performed a subjective evaluation of each trial using VAS (hereinafter referred to as VAS4). At the end of the run, participants performed a subjective evaluation of six trials using VAS (hereinafter referred to as VAS7). Rest periods were inserted before Trial 1 and Trial 4, and after Trial 6.

In the driving practice, participants were instructed to trace a lane of a winding road. Participants' views of the road were rendered according to their steering inputs. The level of the steering parameter used in the practice trial was the same as that in subsequent trials.

In the subjective evaluation practice, participants practiced the subjective VAS7 evaluation by rotating the steering wheel (described later). Table 2 shows all evaluation words we asked participants to use, seven of which were used in VAS7. Six evaluation words, "self-efficacy", "unpleasantness", "pleasantness", "arousal", "expectation", and "excitement" were commonly used in the stiffness and viscosity conditions. The evaluation word "self-efficacy" was selected to ask participants to evaluate how well their steering control matched their intention; that is, how they felt that
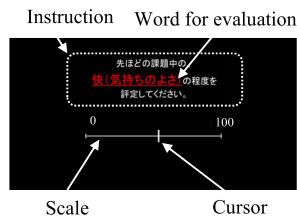
FIGURE 4. Example of the screen of the input interface shown to the participants during the subjective evaluation of performance based on certain descriptive words using a visual analog scale (VAS).

about being able to demonstrate their ability to accomplish the task. We also asked participants to evaluate their valence and arousal [13] while performing the task. The pleasantness and unpleasantness were evaluated separately because we considered the possibility that these factors may not exist on the same axis. The evaluation word "expectation" was selected to ask the participants how well they expected to perform the task. The evaluation word "excitement" (described as "waku-waku" in Japanese) was selected to ask them to gauge how much excitement they felt while performing the task. One word differed between the stiffness and viscosity conditions; we used "anxiety" in the stiffness condition and "motivation" in the viscosity condition. The evaluation word "motivation" in the viscosity condition was selected because we considered that a delay in the response of the vehicle due to an increase in viscosity could decrease a participant's motivation to accurately perform the task. On the other hand, the evaluation word "anxiety" in the stiffness condition was selected because vehicle development engineers have an empirical belief that when the reaction force from the steering wheel is too low, drivers often experience anxiety. In the VAS4 period, participants evaluated their feelings while performing each trial in terms of four evaluation words: "self-efficacy", "pleasantness", "nimbleness", and "smoothness" (Table 2). Two of the four evaluation words ("self-efficacy" and "pleasantness") were commonly seen in the VAS7 evaluations. The remaining two words, "nimbleness" and "smoothness" are generally used by vehicle development engineers to evaluate steering performance.

In VAS7, after the final rest period in each run, participants were asked to perform a subjective evaluation of how they felt during the overall run. At the beginning of VAS7, an instruction for an evaluation word and a VAS scale (Fig. 4) were presented to participants, next they moved the cursor on the scale to the left or right by rotating the steering wheel to score each word. The order of the seven evaluation words was randomized, and the initial position of the cursor for each word was randomized around 50 (near the center of the scale), with a range of ±5 to eliminate the possibility of biasing the rating value by fixing the initial value of the cursor. If the cursor did not move for 2 s, the position was fixed and recorded as the rating score.

For the rest of the phases, a fixation cross was shown at the center of the display (the leftmost display shown in the lowest row in Fig. 3), and participants instructed to look at it.

Each trial consisted of "ready", "countdown", "straight", "gate", score feedback, and subjective evaluation (VAS4) periods. In the ready period, the word "Ready" was displayed for 1 s prior to the start of the countdown period (the second display from the left in the lowest row in Fig. 3). In the countdown period, the number decremented by one every 1 s starting from three; this was shown at the center of the display (the third display from the left in the lowest row in Fig. 3) and disappeared 1 s after the countdown reached 1 s. The vehicle automatically started to move when the timer reached zero. Participants were instructed to prepare for the upcoming task and to imagine how well they would perform a task in which they were required to pass through the center of a gate (described later) as smoothly as possible. In the "straight" period, participants were instructed to trace the white line in the center of the road. In the "gate" period, participants were instructed to control the vehicle to pass through the center of the gate as precisely and smoothly as possible. During this period, five gates were presented one at a time; the first, third, and fifth gates were presented at the center of the road, whereas the second and fourth gates randomly appeared on the left or right side of the white line at the center of the road. In the feedback period, the difference of the x-coordinates between the center of the gate and the position where the center of the car passed through the gate (excluding the first and fifth gates) was calculated. The calculated value was converted to 0-100 and presented to the participants as a feedback score to assess the task performance of the trial. The score was presented for a randomly selected duration of time of 1, 3, or 5 s. After each trial, participants performed subjective evaluations of the last trial (VAS4) in the same manner as in VAS7.

3) STEERING REACTION FORCE CHARACTERISTICS

Fig. 5 shows the steering reaction force characteristics presented to participants. To measure the steering torque using a torque sensor that could not be used in a strong magnetic field in the MRI gantry, the same layout was reproduced outside the MRI scan room. In the reproduced setting, using a steering effort sensor (Model 01184, Sensor Developments Inc. Chelmsford, MA 01824, USA) mounted on the steering wheel, we measured the steering torque relative to the steering angle while performing one run of the driving task. The upper row of Fig. 5 shows that the stiffness parameters changed the slopes of the regression lines but did not affect the hysteresis. The lower row of Fig. 5 shows that the viscosity parameters changed the hysteresis but did not affect the slope of the regression line corresponding to stiffness. These observations confirmed that the parameters in (1) could independently determine the stiffness and viscosity of the steering wheel. The measured value was confirmed to be in agreement with the steering angle output from the steering force sensor attached to the steering wheel within the steering angle and operating speed range shown in Fig. 5.
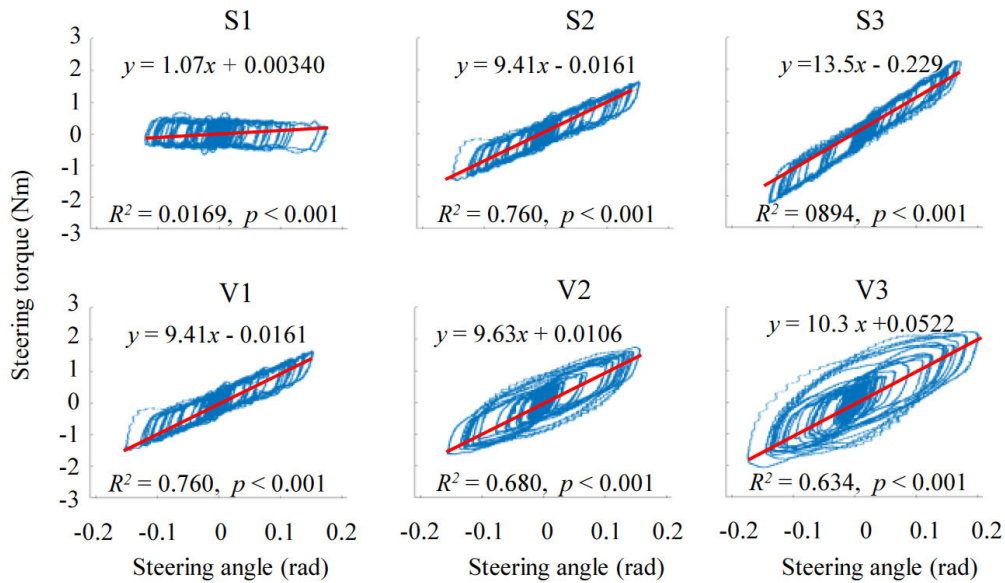
FIGURE 5. Measured steering torques for each stiffness (top row) and viscosity (bottom row) experimental conditions. Prior to the experiment, steering reaction force characteristics were measured by an experimenter outside the magnetic resonance imaging (MRI) scan-room for one run comprised of six trials. The result of the linear regression equation for each condition is shown by a red line.

4) fMRI DATA ACQUISITION

A 3.0 T MRI scanner (MAGNETOM Verio, Siemens AG, Munich, Germany) was used to obtain MRI data. The functional images were acquired using a T2*-weighted gradient echo planar imaging method. The acquisition parameters were as follows: repetition time (TR) = 1,000 ms, echo time (TE) = 30 ms, 42 slices, slice thickness = 3.2 mm (without gaps), voxel size = 3 × 3 × 3.2 mm, flip angle = 80°, and field of view (FOV) = 192 mm. The structural image was acquired using the T1-weighted 3D magnetization-prepared rapid gradient echo imaging method. The acquisition parameters were as follows: TR = 2,500 ms, TE = 2.98 ms, 176 slices, thickness = 1 mm, voxel size = 1 × 1 × 1 mm, flip angle = 9°, and FOV = 192 mm. To reduce head movement caused by steering when using both arms during fMRI measurements, we used a suction-type fixed bag (ESF-19, Engineering System Co., Ltd, Nagano, Japan) in the head coil. In addition, we used a cushion to fill the gap between the head coil and the sides of both ears and the top of the head as much as possible.

5) fMRI DATA ANALYSIS

Data were analyzed using Statistical Parametric Mapping version 12 (SPM12) software (Wellcome Department of Cognitive Neurology, London, UK.) [14]. The first five volumes of functional images obtained in each run were discarded to allow for T1 equilibration; the remaining volumes were analyzed. Spatial correction of the movement of the head was performed based on the first volume (realignment). The T1-weighted structural image for each participant was then aligned to the first volume of the echo-planar images (EPIs)

for the corresponding participant (co-registered) and normalized to the Montreal Neurological Institute (MNI) template.

In this study, it was difficult to regress out the motion parameters based on SPM during measurement of brain activity because the noise caused by the movement of the head associated with the steering wheel operation was very large. Therefore, we modified the Human Connectome Project (HCP) pipeline so that their MultiRunFIX [15] could be applied to data preprocessed by the SPM software. The independent components were extracted by Multi-Run sICA (spatial independent component analysis) from the normalized EPI data, which were concatenated from six runs. The reason for linking the 6-run data is that it is more advantageous to have more time points in order to improve the noise and signal separation performance for sICA. This reduces the risk of removing not only noise but also task-related activities due to low separation performance. To the extracted independent components, automatic labeling based on machine learning was not performed; instead we performed manual labeling based on a study by Griffanti *et al.* [16]. In the last noise component removal step, using the FIX cleanup procedures described by Griffanti *et al.* [15] described later, motion regression was performed using 24 parameters for each signal and noise component, and concatenated data from which the effects of motion artifacts were more effectively removed were obtained. The concatenated data were divided and returned to the data of each run, and the process was then returned to the SPM12 software.

In the cleanup procedures with FIX, the following three steps were performed, similar to that in the "soft" approach described by Griffanti *et al.* [15]: (1) We regressed out the full space of the motion confounds from both the data and all the
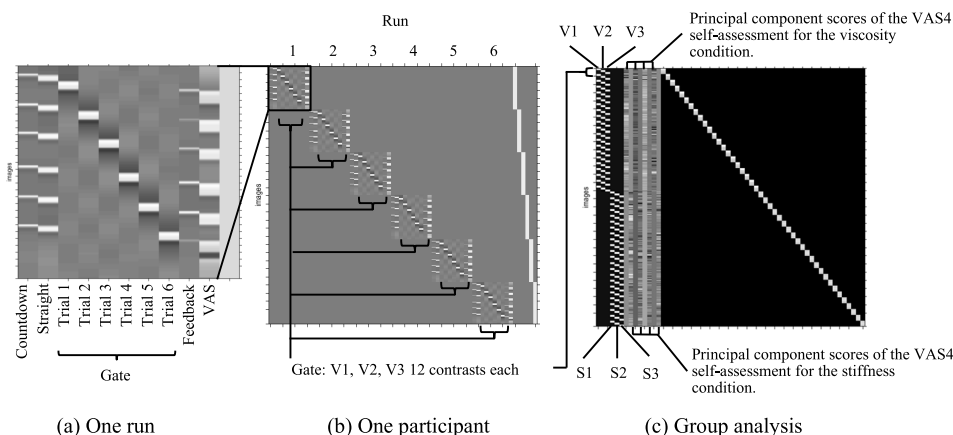
FIGURE 6. Design matrix showing each phase of one run (a), all runs each subject participated in (b), and group analysis (c).

ICA component timeseries; (2) we estimated the contribution of both good and bad components via multiple regression of the data against all (motion-cleaned) ICA timeseries; and (3) the unique contribution of the bad components was removed from the data, employing only the bad ICA components' timeseries and regression coefficients. The 24 parameters used for the above motion regression were motion estimation ($R = [X, Y, Z,$ pitch, yaw, roll$]$), the derivatives (R') of these factors, and their squares (R^2, R'^2).

Following this procedure, the normalized EPIs were smoothed by a Gaussian kernel (full width at half maximum = 8 mm). For pre-processed EPIs, we performed statistical analysis using a general linear model. The "count-down", "straight", "gate," "feedback," and "VAS" periods were modeled as a boxcar function convolved with the canonical hemodynamic response function. Fig. 6 shows an example of the design matrix for the 1st and 2nd level analyses of one run of the "gate" period. In the 1st level analysis, each trial was modeled as one regressor for each run in the "gate" period, and 36 regressors were created for each subject (total of six runs). For each "countdown," "straight," "feedback," and "VAS" period, six trials in each run were modeled as one regressor. Similarly, in the analysis focused on the "countdown" and "straight" periods, we created different design matrices for each; the "countdown" or "straight" period in each trial was modeled as one regressor. For each of the other periods, six trials were modeled as one regressor. A one-way ANOVA within subjects was performed for the 2nd level analysis. To reduce the variance caused by the fluctuations in subjective ratings for each trial, the principal component scores of the VAS4 evaluations after each trial (described below) were adopted as covariates of no interest. Prior to the regression analysis, low-frequency fluctuations in the blood oxygenation level-dependent (BOLD) signal were eliminated by applying a high-pass filter with a cut-off of 128 s. Moreover, serial correlations among scans were estimated using an autoregressive model (AR (1)) to remove high-frequency noise contaminating the EPI time-series. The contrast images for the countdown, "straight",

and "gate" periods were calculated for each participant using the fixed-effects model and were then considered in the group analysis using a random-effects model. The anatomical region was identified using SPM Anatomy toolbox 2.2b (Forschungszentrum Jülich GmbH, Jülich, Germany) [17]–[19] and Talairach Client 2.4.3 (Research Imaging Institute, San Antonio, TX 78229, USA) [20], [21].

6) SUBJECTIVE RATINGS
A principal component analysis (PCA) was performed for the subjective rating data obtained in the stiffness and viscosity conditions. For VAS7, six evaluation words common to both conditions were used in the PCA. One participant rated with extreme values for all evaluation words in most trials in the viscosity condition; this participant gave ratings of 100 in 96.5% of his VAS4 evaluations, and 0 (for anxiety) or 100 (for other words) for 95.2% of his VAS7 evaluations. Thus, we excluded this participant from the analysis because the PC could not be calculated.

III. RESULTS
A. STEERING BEHAVIORS
Fig. 7 shows the time-series of steering angles in each trial. (a) to (d) are examples of sections from Countdown to Gate. Since the appearance of the two gates on the left or right in Fig. 3 is random, there are four possible combinations of gate appearances. Therefore, (a) to (d) represent four selected ways from the six trials of a certain participant. (e) and (f) show the mean and standard deviation of all subjects' trials under all conditions of stiffness and viscous conditions, respectively. Since the gates appear randomly on the left or right, the average and standard deviation between trials were calculated using the absolute value of the steering angle.

B. COMMON BRAIN ACTIVITY IN THE STIFFNESS AND VISCOSITY CONDITIONS
To examine the brain activity related to each period in the driving task, we calculated the signals during the count-down, "straight", and "gate" periods. Fig. 8 shows the
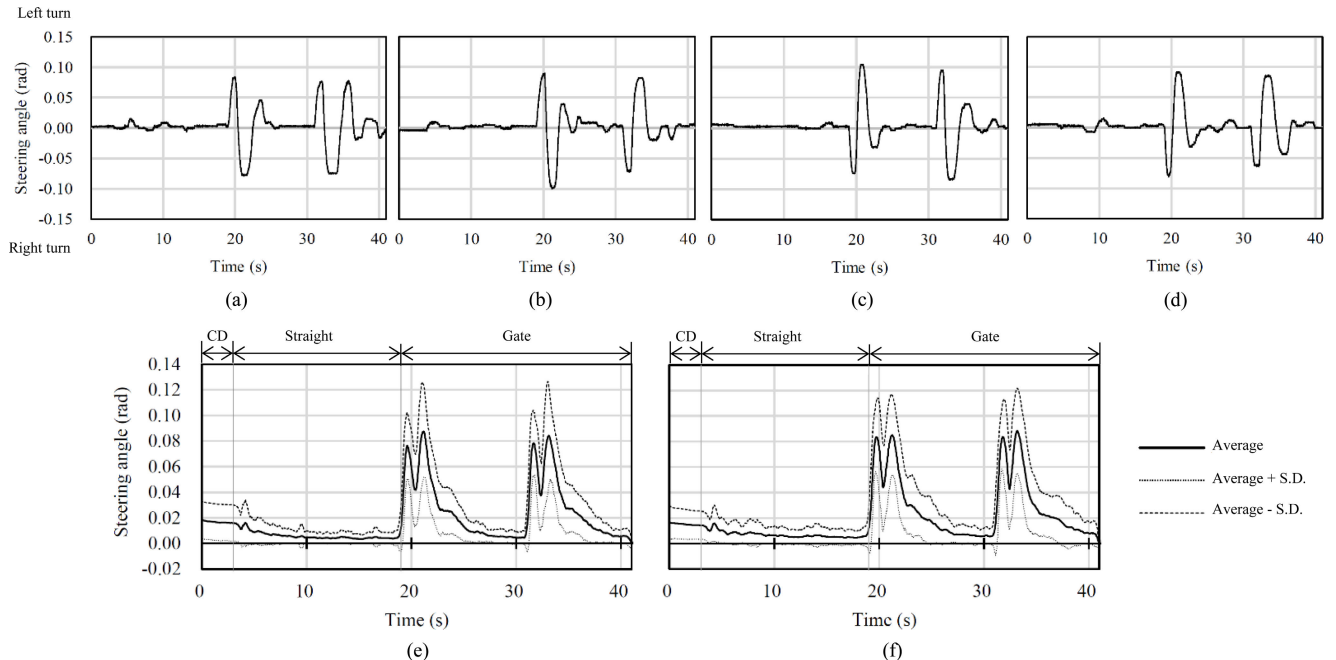
FIGURE 7. Time-series examples of steering angle during the driving task. (a) to (d) are examples of one trial under one viscosity condition (V2). These examples correspond to four patterns of combinations of two gates that appear randomly on the left or right during a single trial. (a) An example of a trial in which both gates appeared on the left. (b) An example of a trial in which the first gate appeared on the left, the second on the right. (c) An example of a trial in which the first gate appeared on the right, the second on the left. (d) An example of a trial in which both gates appeared on the right. (e) and (f) show the average and standard deviation of the absolute values of steering angles over all trials of all subjects for each stiffness and viscosity condition. (e) shows the time series under the stiffness condition, and (f) under the viscosity condition. These measurements were performed with the steering angle meter built in the reaction force generation motor. The measured values showed good agreement with those measured at the steering position under the measurement conditions shown in Fig. 5. CD = Countdown.

FIGURE 8. Brain regions significantly activated at the thresholds of family-wise error (FWE) with a corrected p < 0.05 at the voxel level in the stiffness (top row) and viscosity (bottom row) conditions during the "countdown" (a), "straight" (b), and "gate" (c) periods. BA: Brodmann area, IPL: Inferior parietal lobule, IPS: Intraparietal sulcus, V1: Primary visual, cortex, V2: Secondary visual cortex, V3: Tertiary visual cortex, V4: Quaternary visual cortex, V5/MT: Middle temporal visual area, Hem: Hemisphere, Verm: Vermis.
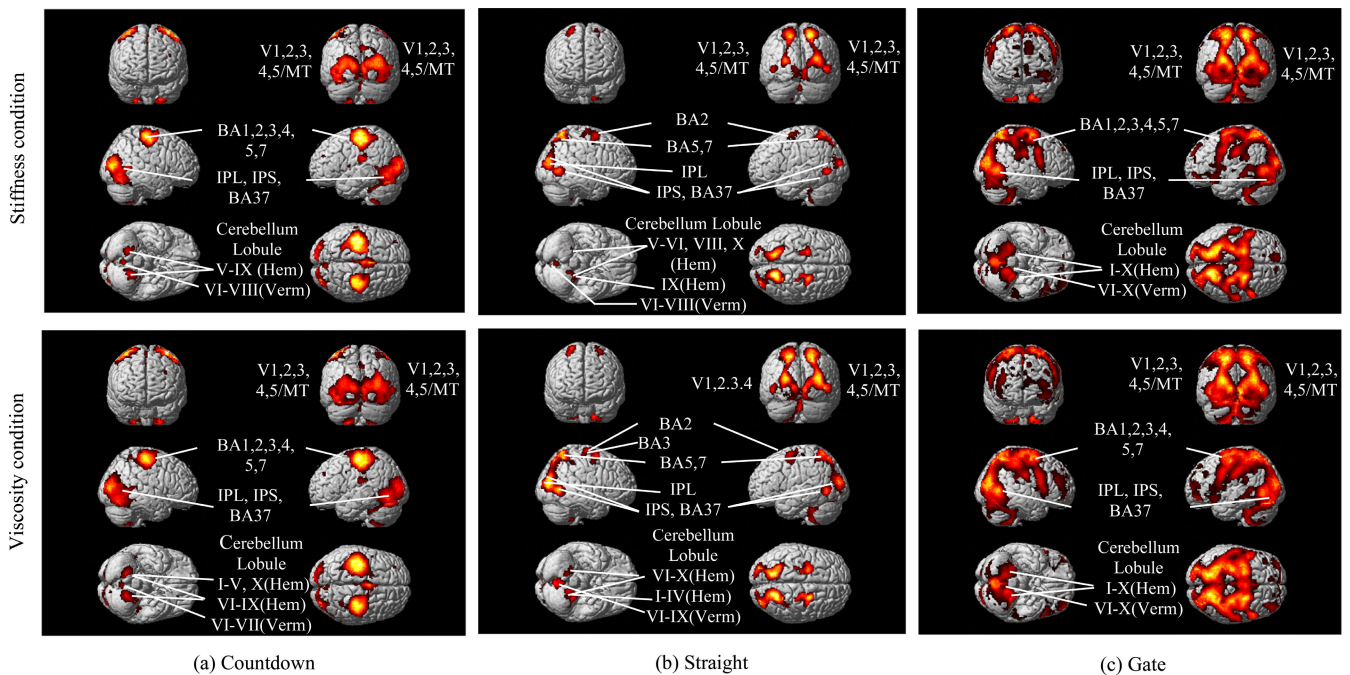
brain regions that exhibited significant activations at the thresholds of family-wise error (FWE) with a corrected $p < 0.05$ at the voxel level in the stiffness and viscosity conditions during the countdown, "straight", and "gate" periods. We performed FWE corrections for each predefined contrast. The MNI coordinates of activation clusters are
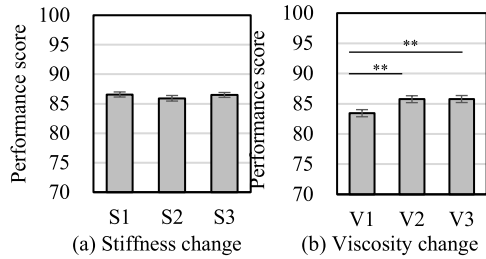
FIGURE 9. Performance scores for each of the three stiffness (a) and viscosity (b) condition parameters. **: p < 0.01. Error bar: SEM.

shown in Appendix Table 3 and Appendix Table 4. In both stiffness and viscosity conditions, we found significant activations in the visual cortex, somatosensory area, primary motor area, somatosensory association area, and cerebellum during the countdown period. During the "straight" period, we found significant activations in the visual cortex, somatosensory area, somatosensory association area, and cerebellum. During the "gate" period, we found significant activations in the visual cortex, somatosensory area, primary motor area, somatosensory association area, and cerebellum.

C. SUBJECTIVE RATINGS AND PERFORMANCE SCORES

Fig. 9 shows the performance scores of the task that indicate how close to the center of the gate the participants were able to pass through. A repeated measures ANOVA revealed no significant main effect of the levels in the stiffness condition ($F (2, 22) = 0.601$, $p = 0.549$), but a significant main effect of the levels in the viscosity condition ($F (2, 21) = 13.344$, $p < 0.01$).

Fig. 10 shows the result of the subjective evaluations obtained from VAS4 (for each trial). Fig. 10 (a) shows the mean rating scores for each evaluation word under the stiffness condition, and Fig. 10 (b) shows those under the viscosity condition. Under the stiffness condition, a repeated measures ANOVA with levels of stiffness as a factor revealed a significant main effect for all evaluation words, including "self-efficacy" ($F (2, 22) = 51.384$, $p < 0.01$), "pleasantness" ($F (2, 22) = 21.699$, $p < 0.01$), "nimbleness" ($F (2, 22) = 38.777$, $p < 0.01$), and "smoothness" ($F (2, 22) = 28.601$, $p < 0.01$). Under the viscosity condition, a repeated measures ANOVA revealed no significant main effect of levels of viscosity for any evaluation words, "self-efficacy" ($F (2, 20) = 2.424$, $p = 0.089$), "pleasantness" $F (2, 20) = 0.575$, $p = 0.563$), "nimbleness" ($F (2, 20) = 1.084$, $p = 0.339$), and "smoothness" ($F (2, 20) = 2.109$, $p = 0.122$). The results of Tukey's post-hoc tests comparing the levels in each condition are shown in the figure.

Fig. 10 (c) shows the factor loadings of each PC for each evaluation word and the contributions for each PC obtained by the PCA. The subjective rating data obtained from VAS4 (for each trial) for the stiffness and viscosity conditions were analyzed by PCA. The factor loading of the first PC was
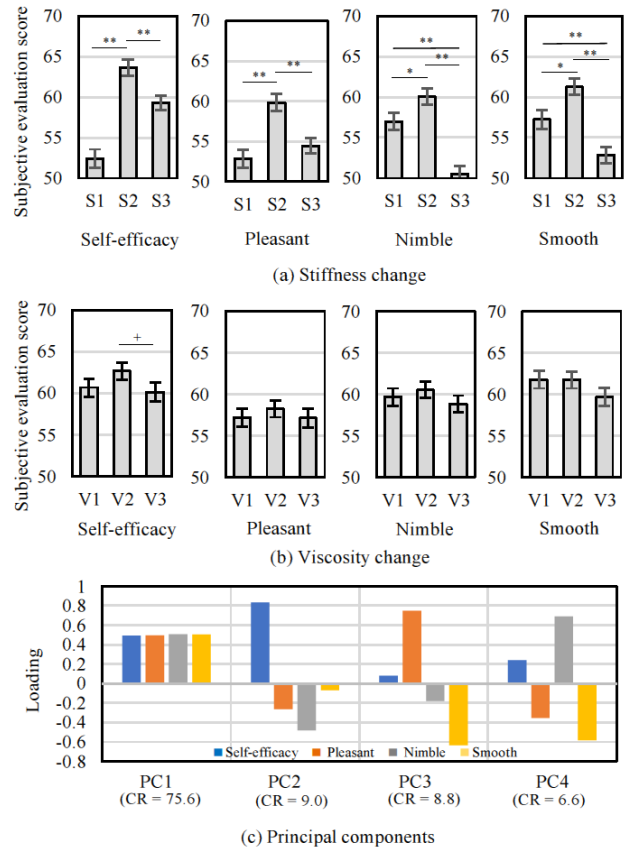

FIGURE 10. VAS4 subjective evaluation scores for trials based on a visual analog scale (VAS) for each descriptive word for stiffness (a) and viscosity (b) conditions. The factor loading and contribution ratios for each principal component based on descriptive words are shown in (c). **: p < 0.01, *: p < 0.05, +: p < 0.1, Error bar: SEM. CR: Contribution ratio.

positive for evaluation words related to a positive affective state. Therefore, this PC can be interpreted as being a component reflecting positive feelings. The second PC reflected high self-efficacy with low nimbleness. The third PC reflected a feeling of comfort associated with low smoothness. The fourth PC was related to maneuverability, with high nimbleness and low smoothness.

The results of the analyses of VAS7 ratings (for each run) are shown in Fig. 11. Fig. 11 (a) shows the mean rating scores for each evaluation word under the stiffness condition, and (b) those under the viscosity condition. Under the stiffness condition, a repeated measures ANOVA with stiffness level as a factor revealed a significant main effect for four words: "anxiety," "self-efficacy," "pleasantness," and "excitement" ("unpleasantness" ($F (2, 22) = 0.846$, $p = 0.433$), "anxiety" ($F (2, 22) = 6.474$, $p < 0.01$), "self-efficacy" ($F (2, 22) = 16.240$, $p < 0.01$), "pleasantness" ($F (2, 22) = 5.925$ $p < 0.01$), "arousal" ($F (2, 22) = 2.676$, $p = 0.076$), "expectation" ($F (2, 22) = 4.562$, $p = 0.014$), and "excitement" ($F (2, 22) = 8.971$, $p < 0.01$). Under the viscosity condition, a repeated measures ANOVA revealed no significant main effect of viscosity levels for any evaluation words ("unpleasantness" ($F (2, 20) = 0.045$, $p = 0.956$),
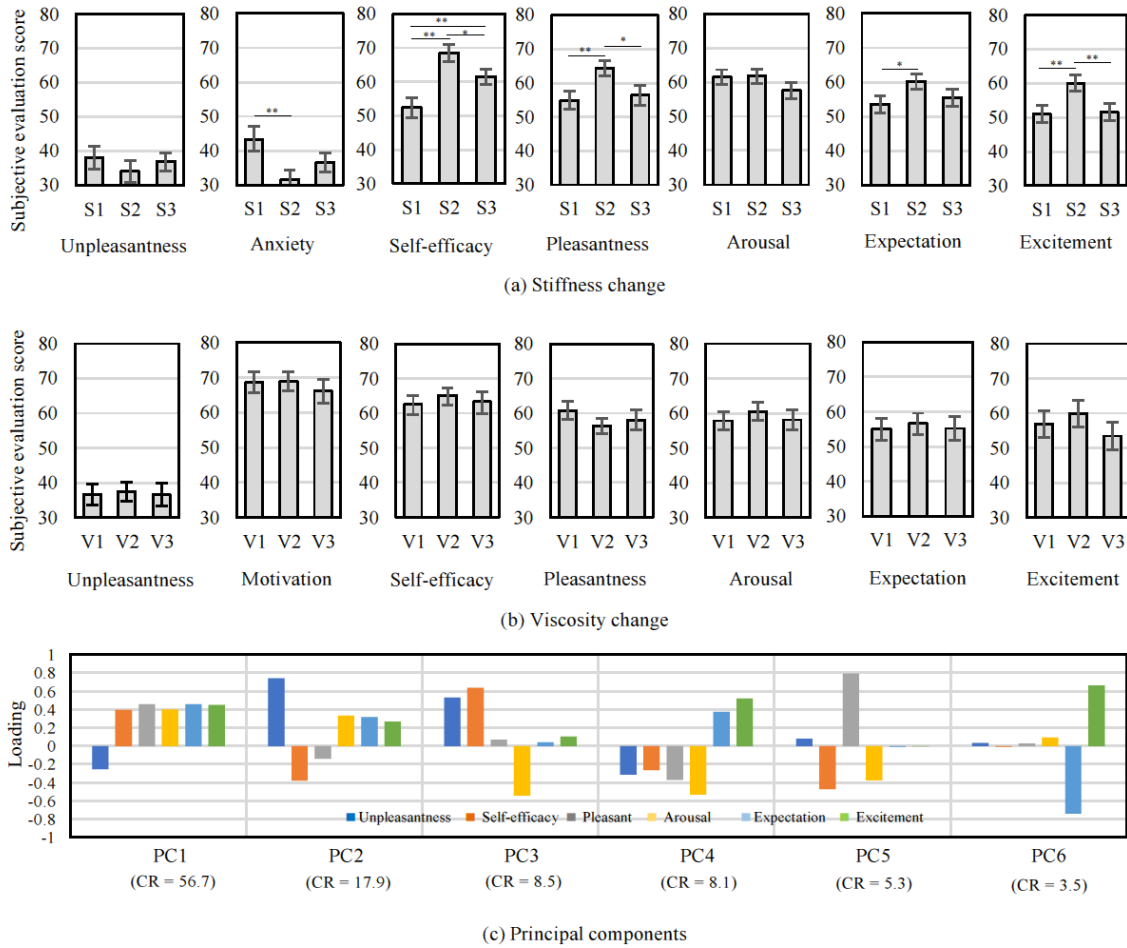
FIGURE 11. VAS7 subjective evaluation scores at the end of the run based on a visual analog scale (VAS) for each descriptive word for the stiffness (a) and viscosity (b) conditions. The factor loadings and contribution ratios for each principal component based on the descriptive words are shown in (c). **: p < 0.01, *: p < 0.05, Error bar: SEM. CR: Contribution ratio.

"anxiety" (F (2, 20) = 0.601, p = 0.552), "self-efficacy" (F (2, 20) = 0.536, p = 0.588), "pleasantness" (F (2,20) = 1.071 p = 0.349), "arousal" (F (2, 20) = 0.497, p = 0.611), "expectation" (F (2, 20) = 0.165, p = 0.848), and "excitement" (F (2, 20) = 1.701, p = 0.191)). The results of Tukey's post-hoc tests comparing the levels in each condition are shown in Fig. 11 (a).

Fig. 11 (c) shows the factor loadings of each PC for each evaluation word and the contributions for each PC obtained by PCA. For the subjective ratings for each run (VAS7), we performed PCA using six evaluation words common in the stiffness and viscosity conditions. In the subjective ratings for each trial and for each session, the factor loading of the first PC was positive for evaluation words related to a positive affective state (except for discomfort), but negative only for "discomfort" related to a negative affective state. Therefore, the first PC can be interpreted as a component reflecting positive feelings. For subjective evaluations of each session, the second PC meant that participants had a high level of discomfort, with low self-efficacy. The third PC reflected a high self-efficacy, but a high degree of discomfort and

low arousal, while the fourth PC reflected high expectation and excitement, the fifth a high degree of pleasantness but low self-efficacy and arousal, and the sixth a degree of high excitement and low expectation.

To examine the correlation between subjective ratings (VAS4) and performance scores, we performed regression analyses with ratings for each evaluation word as the objective variable and performance score as the explanatory variable. Under the stiffness condition, regression analyses revealed significant relationships between performance scores and the ratings of evaluation words, including "self-efficacy" (R^2 = 0.100, β = 0.769, t = 9.581, F (1, 826) = 91.804, p < 0.01), "pleasantness" (R^2 = 0.118, β = 0.834, t = 10.512, F (1, 826) = 110.495, p < 0.01), "nimbleness" (R^2 = 0.079, β = 0.664, t = 8.415, F (1, 826) = 70.819, p < 0.01), and "smoothness" (R^2 = 0.114, β = 0.829, t = 10.299, F (1, 826) = 106.073, p < 0.01). Under the viscosity condition, regression analyses revealed significant relationships between performance scores and the ratings of evaluation words, including "self-efficacy" (R^2 = 0.095, β = 0.558, t = 8.880, F (1, 754) = 78.846, p < 0.01),

FIGURE 12. (a) Significant brain activation in the contrast of S3 > S1 in the stiffness condition during the gate period at the threshold of family-wise error (FWE) with a corrected $p < 0.05$ at the voxel level. The blue rectangles indicate a left motor cortex cluster containing the Montreal Neurological Institute (MNI) coordinates −48, −24, 62. (b) Percent signal change in the activated cluster in the contrast of S3 > S1. (c) Spatial relationship between activation peaks observed at MNI coordinates: −48, −24, 62 and the central sulcus. **: $p < 0.01$, *: $p < 0.05$, Error bar: SEM.
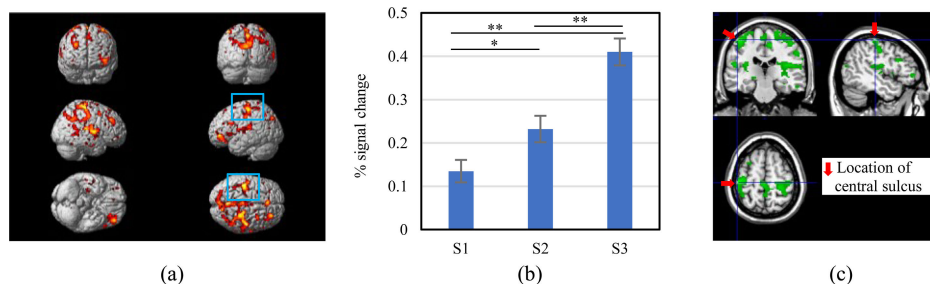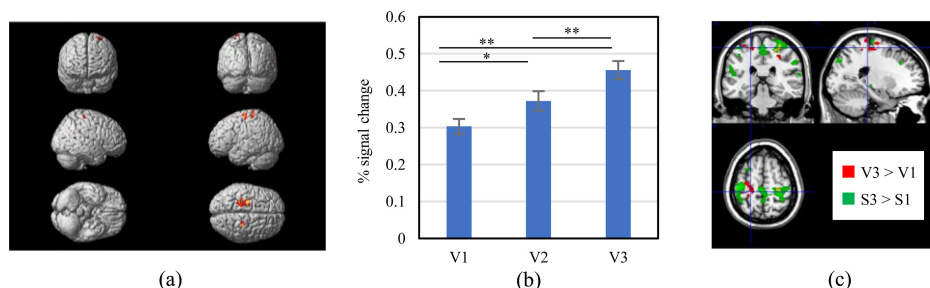

FIGURE 13. (a) Significant brain activation in the contrast of V3 > V1 in the viscosity condition during the gate period at the threshold of family-wise error (FWE) with a corrected $p < 0.05$ at the peak level. (b) Percent signal change in the contrast of V3 > V1. (c) Spatial relationship between significant activation in the contrast of V3 > V1 with the peak activation in the left premotor cluster including the Montreal Neurological Institute (MNI) coordinates −22, −30, 62 and the significant activation in the contrast of S3 > S1. **: $p < 0.01$, *: $p < 0.05$, Error bar: SEM.

"pleasantness" ($R^2 = 0.043$, $\beta = 0.365$, $t = 5.794$, $F(1, 754) = 33.569$, $p < 0.01$), "nimbleness" ($R^2 = 0.064$, $\beta = 0.425$, $t = 7.205$, $F(1, 754) = 51.916$, $p < 0.01$), and "smoothness" ($R^2 = 0.079$, $\beta = 0.501$, $t = 8.066$, $F(1, 754) = 65.058$, $p < 0.01$).

Overall, these results showed significant correlations between subjective evaluations and objective performance scores. This suggests that the subjective ratings reflected not only the participants' mental state during steering, but also that the steering performance scores fed back to affect perceptions of performance after the steering trials ended. These confounders are possibly associated with brain activation related to subjective ratings. Therefore, we did not examine the relationship between the subjective ratings and brain activity.

D. BRAIN ACTIVITY CORRELATED WITH PHYSICAL PARAMETERS

To examine the brain regions showing activity depending on stiffness and viscosity parameters, we compared the brain activity between S3 and S1 and also between V3 and V1 during the "gate" period.

We performed FWE corrections for each predefined contrast for both stiffness and viscosity. A significant effect of stiffness was observed in the somatomotor and sensorimotor cortices at the threshold of FWE with a corrected $p < 0.05$ at the voxel level (Fig. 12 (a)). In the left primary motor cortex (M1), we found a cluster shown in the blue rectangles with peak activation occurring at MNI coordinates −48, −24, 62, corresponding to the location of the central sulcus opening near a region suggested to be involved in controlling movement of the wrist by Germann *et al.* [22]. The MNI coordinates of this cluster are shown in Appendix Table 5. Fig. 12 (b) shows the percent signal change of this left M1 cluster for each stiffness level. Fig. 12 (c) shows the spatial relationship between the peak activation observed at MNI coordinates −48, −24, 62 and the central sulcus.

A significant effect of viscosity was observed in the somatomotor and sensorimotor cortices at the threshold of FWE with a corrected $p < 0.05$ at the voxel level (Fig. 13 (a)). One of the three significantly activated clusters included the left premotor cortex with a peak activation at MNI coordinates −26, −18, 58. The MNI coordinates of this cluster are shown in Appendix Table 6. In Fig. 13(b), the percent signal change in the activation of a cluster at MNI coordinates −22, −30, 62 for each viscosity level is shown relative to the cluster shown in Fig. 13(a). This area is involved in controlling movement of the shoulder, as reported by Colebatch *et al.* [23]. Fig. 13(c) shows the spatial relationship between significant activation in the contrasts of V3 > V1 and

S3 > S1 with the peak activation in the left premotor cluster with MNI coordinates of $-22, -30, 62$.

IV. DISCUSSION

A. VALIDITY OF fMRI DATA

In the "countdown," "straight," and "gate" periods, it was predicted that there would be activation in the brain regions involved in task-related visual and motor processing; indeed, these periods were associated with significant activation in the visual cortex (see Fig. 8). In the "countdown" period, we observed activations in the visual cortices, somatosensory areas, primary motor area, parietal somatosensory association area, and cerebellum. During this period, participants were required to prepare for the upcoming task by grasping the steering wheel and viewing the countdown numbers. Processing in this task would require motor planning and the sensory perception necessary for grasping the steering wheel. This result was consistent with our prediction.

In the "straight" period, we observed activations in the primary somatosensory cortex, parietal somatosensory association area, and cerebellum, as well as the visual cortices. This result can be interpreted as force modulation based on the processing of visual information (e.g., [24]), since the participants were required to maintain a constant force on the steering wheel to trace the straight white line.

During the "gate" period, participants performed a kind of a visuomotor task in which they needed to steer and maintain control of the virtual vehicle to pass through the center of the gates. This led to the prediction that the brain regions involved in motor and visual processing would be engaged because the task would require the coordination of both hands in accordance with the timing of the car's passage through the gate. This task required the participant to process sensorimotor information based on the steering reaction force and visual information. The brain regions activated during the "gate" period included the parieto-motor regions and the cerebellum. Engagement of these regions is consistent with those reported in a study by Kan *et al.* [10] in which they used an fMRI-compatible driving simulator, requiring participants to make a turn. This suggests that similar cognitive resources associated with visuospatial and motor coordination were recruited in the "gate" period in our study as those activated when making a turn. The activations observed in various brain regions in each period of the task can be reasonably interpreted based on the predicted functional requirement for performance in each period.

Since more brain regions were active in the contrasts of S3 > S1 than in that of V3 > V1 (see Figs. 12 and 13), a change in the stiffness condition had greater effects on brain activity than changes in the viscosity condition. This is supported by the fact that in the stiffness condition, many evaluation words had a significant main effect ($p < 0.01$), whereas in the viscosity condition, no evaluation words showed a significant main effect (see Figs. 10 and 11). Therefore, the range of affective changes in the participants was larger under the stiffness condition than under the viscosity condition. In future studies, we plan to examine the relationship between subjective evaluation and brain activity by dissociating participants' mental state during steering and brain activation from other factors, such as the steering performance scores fed back after the end of the steering trials.

B. BRAIN ACTIVITY CORRELATED WITH VISCOELASTIC CONDITIONS

We found that changes in stiffness covaried with changes in activation in the M1 region associated with the hand representation (inverted omega sign, Yousry *et al.* [25]) (Fig. 12). Functional neuroimaging studies revealed somatomotor body representation of the M1 region, including distal representation in the ventral portion of M1 and proximal representation in the dorsal portion of M1 (Colebatch *et al.* [23]; Grafton *et al.* [26]). The well-known morphological sign for the hand region (distal representation) is the inverted omega sign (Yousry *et al.* [25]). Recently, Germann *et al.* [22] showed that the central sulcus is composed of five distinct sulcal segments and that each segment relates systematically to the sensorimotor representation of distinct parts of the body. Thus, stiffness of the wheel is mainly associated with driving control mediated by the distal muscles (i.e., the hand).

In contrast, changes in viscosity covaried with driving-related activation in the dorsal premotor cortex and the dorsal M1 region associated with hand representation (Fig. 13). According to Germann *et al.* [22], the precentral gyrus dorsal to the hand area with the inverted omega sign represents the proximal muscles. Studies involving lesions of the dorsal premotor cortex showed weakness of the contralateral shoulder or hip muscles, and uncoordination of movements requiring temporal adjustment between proximal muscle activations on both sides of the body (limb-kinetic apraxia) (Freund [27]). Thus, viscosity affects driving control mediated by the proximal muscles.

The mechanical characteristics of the steering reaction force in the experiment reflected that of a quadratic linear system (i.e., a spring-mass-damper system, with the torque input and the angle output consisting of inertia, stiffness and viscosity parameters). In this case, the damping ratio decreases as the stiffness increases, and, conversely, increases as the viscosity increases. Also, the natural angular frequency increases in proportion to the square root of the stiffness (e.g., [28]). Therefore, a steering system has a quicker response when the stiffness becomes larger, thus requiring distal force tuning. On the other hand, the system has a slower response when the viscosity becomes larger, thus requiring proximal force tuning.

In this study, we demonstrated for the first time that distinct parameters representing the physical characteristics of the steering wheel, namely stiffness and viscosity, can affect vehicular control during driving by engaging different muscular systems.

From the viewpoint of human physical characteristics, the forearms and hands are operated by distal muscles and

TABLE 3. Location and volume of active clusters in the stiffness condition. Brain regions significantly activated at the family-wise error (FWE) thresholds with a corrected p < 0.05 at the voxel level.

(a) Countdown period

Region	Area	X (mm)	Y (mm)	Z (mm)	Peak Z	Voxels
L Postcentral Gyrus	3b	−42	−22	58	Inf	4295
L Precentral Gyrus	6	−36	−20	70	Inf	
L Rolandic Operculum		−44	−24	22	7.49	
L Superior Parietal Lobule	5L (SPL)	−28	−46	56	6.61	
R Middle Occipital Gyrus	hOc4lp	32	−86	10	Inf	14074
R Calcarine Gyrus	hOc1 [V1]	12	−80	6	Inf	
L Superior Occipital Gyrus	hOc1 [V1]	−8	−98	4	Inf	
R Cuneus	hOc2 [V2]	14	−94	14	Inf	
L Calcarine Gyrus	hOc1 [V1]	−10	−82	2	Inf	
R Cerebelum (IV-V)	Lobule VI (Hem)	24	−50	−18	Inf	
L Cerebelum (IV-V)	Lobule VI (Hem)	−26	−46	−22	Inf	
L Middle Occipital Gyrus	hOc4lp	−28	−90	8	Inf	
L Inferior Occipital Gyrus	19	−42	−66	−8	Inf	
L Superior Occipital Gyrus	hOc4d [V3A]	−16	−94	18	Inf	
L Fusiform Gyrus	hFG1	−32	−60	−14	Inf	
L Lingual Gyrus	18	16	−74	−6	Inf	
R Occipital Fusiform Gyrus	37	26	−70	−12	Inf	
R Lingual Gyrus	18	−16	−72	−10	Inf	
L Calcarine Cortex	18	−6	−92	−4	Inf	
R Inferior Occipital gyrus	37	50	−70	−8	6.99	
R Precentral Gyrus	38	−26	70	Inf	2246	
R Precentral Gyrus	4	40	−18	54	Inf	
R Precentral Gyrus	4	36	−26	58	Inf	
R Precentral Gyrus	6	46	−18	62	Inf	
R Precentral Gyrus	6	30	−20	68	Inf	
R Superior Frontal Gyrus	6	32	−4	68	Inf	
R Superior Frontal Gyrus		36	−8	66	Inf	
R Precentral Gyrus		40	−6	62	7.67	
L Posterior-Medial Frontal	6	−2	−2	54	Inf	2316
L MCC	5	−10	−26	48	Inf	
L Posterior-Medial Frontal	6	−6	−18	50	Inf	
R MCC	6	12	−24	46	7.76	
L MCC	5M (SPL)	−12	−38	52	6.39	
R Cerebelum (VIII)	Lobule VIIIb (Hem)	20	−56	−56	7.58	249
L Cerebelum (VIII)	Lobule VIIIb (Hem)	−22	−48	−56	6.46	323
L Cerebelum (VIII)	Lobule VIIIb (Hem)	−28	−42	−54	6.25	
Cerebellar Vermis (6)	Lobule VI (Verm)	0	−60	−22	6.43	241
Cerebellar Vermis (8)	Lobule VIIIa (Verm)	2	−64	−32	5.98	
L Thalamus	Thal: Prefrontal	−14	−20	8	5.50	34
L Rolandic Operculum	6	−46	0	8	5.32	27
L Middle Frontal Gyrus	10	−38	46	28	5.06	17
R Lingual Gyrus	36	12	−40	−2	4.63	3
L Putamen		−14	10	−10	4.63	2
R Caudate Nucleus		16	16	−10	4.62	1
L Superior Parietal Lobule	7	−16	−68	46	4.60	7

(b) Straight period

Region	Area	X (mm)	Y (mm)	Z (mm)	Peak Z	Voxels
R Superior Parietal Lobule	7A (SPL)	18	−60	60	Inf	4848
R Superior Occipital Gyrus	19	28	−84	20	Inf	
R Middle Temporal Gyrus	19	44	−64	0	Inf	
R Lingual Gyrus	hOc3v [V3v]	14	−76	−8	Inf	
L Lingual Gyrus	hOc3v [V3v]	−12	−80	−8	Inf	
L Lingual Gyrus	hOc1 [V1]	−10	−84	−2	Inf	
R Superior Occipital Gyrus	7	26	−72	34	Inf	
R Superior Parietal Lobule	7P (SPL)	22	−78	50	5.74	
Cerebellar Vermis (6)	Lobule V (Hem)	0	−62	−20	5.71	
Cerebellar Vermis (6)	Lobule VI (Verm)	2	−70	−14	5.43	
L Superior Parietal Lobule	7A (SPL)	−18	−60	58	Inf	1979
L Superior Parietal Lobule	7A (SPL)	−20	−56	56	Inf	
L Precuneus	7A (SPL)	−14	−62	70	Inf	
L Middle Occipital Gyrus	19	−24	−84	14	Inf	
L Superior Parietal Lobule	7A (SPL)	−16	−78	52	7.61	
L Middle Occipital Gyrus	7	−26	−66	28	6.10	
L Middle Occipital Gyrus	19	−42	−66	0	Inf	342
RPrecentral Gyrus	6	30	−6	52	Inf	862
R Superior Frontal Gyrus	6	24	0	62	Inf	
RPrecentral Gyrus		28	−22	60	7.67	
R Superior Frontal Gyrus	6	20	−14	76	7.64	
R Superior Frontal Gyrus	6	20	−14	66	7.22	
L Superior Frontal Gyrus	6	−22	−4	54	Inf	617
L Cerebelum (IX)	Lobule VIIIb (Hem)	−16	−48	−50	7.48	188
L Cerebelum (VIII)	Lobule X (Hem)	−22	−36	−48	6.71	
L Cerebelum (VIII)	Lobule VIIIb (Hem)	−28	−40	−50	6.00	
L Cerebelum (VI)	Lobule VI (Hem)	−30	−36	−36	5.85	
L Cerebelum (VI)	Lobule VI (Hem)	−32	−40	−32	5.83	
L Cerebelum (VIII)	Lobule VIIIa (Hem)	−32	−42	−50	5.32	
L Cerebelum (X)	Lobule V (Hem)	−26	−32	−40	5.27	
Cerebellar Vermis (8)	Lobule VIIIa (Verm)	0	−70	−34	7.36	101
R Cerebelum (VIII)	Lobule VIIIb (Hem)	28	−42	−48	4.95	11
L Superior Occipital Gyrus	hOc2 [V2]	−8	−98	8	4.94	2
L Precentral Gyrus		−26	−22	58	4.82	5
L Precentral Gyrus	6	−56	6	38	4.68	3

(c) Gate period

Region	Area	X (mm)	Y (mm)	Z (mm)	Peak Z	Voxels
R Superior Parietal Lobule	7A (SPL)	18	−60	60	Inf	49362
R Superior Occipital Gyrus	19	26	−84	20	Inf	
R Lingual Gyrus	hOc2 [V2]	12	−78	−6	Inf	
L Lingual Gyrus	hOc3v [V3v]	−8	−82	−8	Inf	
R Superior Occipital Gyrus	hOc4d [V3A]	22	−88	16	Inf	
R Cuneus	18	18	−92	12	Inf	
L Middle Occipital Gyrus	hOc4d [V3A]	−20	−90	16	Inf	
L Superior Parietal Lobule	7A (SPL)	−16	−60	60	Inf	
L Superior Parietal Lobule	5L (SPL)	−26	−50	56	Inf	
R Middle Temporal Gyrus	hOc5 [V5/MT]	46	−64	0	Inf	
R Middle Temporal Gyrus	hOc5 [V5/MT]	44	−68	0	Inf	
L Inferior Occipital Gyrus	19	−42	−68	2	Inf	
R Superior Frontal Gyrus	6	24	−2	62	Inf	
L Superior Parietal Lobule	7	−18	−68	44	Inf	
L Superior Frontal Gyrus	6	−22	−4	62	Inf	
L Superior Frontal Gyrus	6	−24	−4	54	Inf	
L Thalamus	Thal: Prefrontal	−12	−20	10	Inf	999
L Putamen		−24	−6	8	6.08	
L Thalamus	Thal: Prefrontal	−8	−24	−2	5.81	
N/A	Thal: Prefrontal	−18	−6	6	5.81	
L Thalamus	Thal: Prefrontal	−14	−8	−2	5.39	
L Superior Medial Gyrus	9	−8	58	34	Inf	299
L Superior Frontal Gyrus		−12	52	42	6.81	
L Superior Frontal Gyrus	8	−12	44	46	6.00	
R Thalamus	Thal: Prefrontal	12	−18	8	Inf	570
R Putamen		28	−12	6	7.46	
L Superior Medial Gyrus	Fp2	−8	56	2	6.51	105
L ACC	Fp2	−6	54	−2	6.33	
L Mid Orbital Gyrus	Fp2	−10	50	−10	5.91	
R Superior Orbital Gyrus	11	14	54	−14	6.50	41
R Superior Medial Gyrus	Fp2	12	58	0	5.69	
R Superior Medial Gyrus	9	8	54	40	5.84	45
R Caudate Nucleus		4	8	−4	5.80	36
N/A		4	2	−6	5.28	
R Caudate Nucleus		10	16	−6	5.07	
N/A		−4	4	−4	4.96	
L Superior Frontal Gyrus	8	−14	30	58	5.66	16
L Middle Frontal Gyrus	10	−32	54	24	5.63	37
L Middle Frontal Gyrus	10	−38	52	14	4.89	
R Insula Lobe	13	34	20	10	5.44	13
R Middle Orbital Gyrus	10	38	48	−14	5.28	6
L Middle Temporal Gyrus	TE 3	−62	−16	0	5.07	11
R Superior Frontal Gyrus	8	14	36	50	4.88	7
NA	Thal: Parietal	20	−26	−4	4.87	7
L Insula Lobe		−30	18	10	4.80	6
R Middle Orbital Gyrus	10	44	50	−12	4.79	2
NA		20	−14	−6	4.67	2
R IFG (p. Orbitalis)	47	38	26	−18	4.58	1
L IFG (p. Triangularis)		−48	38	22	4.57	2
L PCC		0	−44	28	4.51	1
L Caudate Nucleus		−14	24	−8	4.50	1

TABLE 4. Location and volume of active clusters in the viscosity condition. Brain regions significantly activated at the family-wise error (FWE) thresholds with a corrected p < 0.05 at the voxel level.

(a) Countdown period

Region	Area	X (mm)	Y (mm)	Z (mm)	Peak Z	Voxels
L Postcentral Gyrus	3b	-42	-20	56	Inf	4188
L Precentral Gyrus	6	-40	-18	66	Inf	
L Precentral Gyrus	6	-32	-20	64	Inf	
L Superior Frontal Gyrus		-18	4	72	5.69	
L Superior Frontal Gyrus	6	-24	0	70	5.62	
L Superior Parietal Lobule	7PC (SPL)	-26	-54	60	4.67	
R Middle Occipital Gyrus	hOc4lp	32	-86	10	Inf	15964
R Calcarine Gyrus	hOc1 [V1]	14	-80	4	Inf	
R Cuneus	hOc2 [V2]	14	-94	10	Inf	
L Superior Occipital Gyrus	hOc1 [V1]	-8	-98	6	Inf	
L Calcarine Gyrus	hOc1 [V1]	-10	-82	2	Inf	
R Cuneus	hOc1 [V1]	16	-96	6	Inf	
R Cerebelum (VI)	Lobule VI (Hem)	26	-52	-20	Inf	
L Inferior Occipital Gyrus	FG2	-44	-64	-12	Inf	
R Fusiform Gyrus	FG1	30	-64	-16	Inf	
L Inferior Occipital Gyrus	FG2	-40	-70	-12	Inf	
L Fusiform Gyrus	FG1	-34	-62	-16	Inf	
R Cuneus	18	16	-72	-6	Inf	
L Lingual Gyrus	18	-16	-74	-10	Inf	
L Cerebellum Exterior		-20	-56	-18	Inf	
R Temporal lobe	37	40	-60	-16	Inf	
L Middle Occipital Gyrus	19	-30	-82	16	Inf	
R Precentral Gyrus	6	38	-20	64	Inf	2983
R Precentral Gyrus	6	30	-22	74	Inf	
R Precentral Gyrus	6	30	-18	72	Inf	
R Superior Parietal Lobule	7PC (SPL)	32	-50	64	5.61	1868
L Posterior-Medial Frontal	6	-2	-2	52	Inf	
R Posterior-Medial Frontal	6	10	-22	48	7.10	
L MCC	31	-8	-26	48	7.06	
L Posterior-Medial Frontal	6	-6	-22	50	6.85	
L MCC	5M (SPL)	-14	-40	50	5.65	
R Paracentral Lobule	5	16	-40	50	5.43	
L Posterior-Medial Frontal	6	-2	-4	70	5.07	
R Cerebelum (VIII)	Lobule VIIIb (Hem)	22	-54	-56	Inf	330
L Cerebelum (VIII)	Lobule VIIIb (Hem)	-22	-52	-58	Inf	506
L Cerebelum (VIII)	Lobule VIIIb (Hem)	-26	-44	-56	Inf	
L Rolandic Operculum		-48	-22	22	7.53	266
L Lingual Gyrus		-8	-42	2	6.23	90
R Lingual Gyrus	36	10	-40	0	6.01	92
R Calcarine Gyrus	18	18	-52	4	5.86	102
R Lingual Gyrus	hOc1 [V1]	8	-56	8	5.15	
L Middle Frontal Gyrus	10	-32	44	34	5.68	24
L Rolandic Operculum	6	-42	-2	12	5.29	19
L Thalamus	Thal: Prefrontal	-16	-22	8	4.84	7
L Precentral Gyrus	6	-52	4	36	4.80	8
L Middle Orbital Gyrus	Fo3	-20	36	-16	4.70	4
L Precuneus	5M (SPL)	0	-52	62	4.69	4
R Putamen		16	14	-8	4.67	6

(b) Straight period

Region	Area	X (mm)	Y (mm)	Z (mm)	Peak Z	Voxels
L Lingual Gyrus	Area hOc1 [V1]	-10	-86	-2	Inf	10956
R Superior Parietal Lobule	Area 7A (SPL)	22	-58	56	Inf	
R Middle Occipital Gyrus	19	34	-84	14	Inf	
L Superior Parietal Lobule	Area 7A (SPL)	-16	-64	54	Inf	
R Middle Temporal Gyrus	39	42	-64	2	Inf	
R Calcarine Gyrus	Area hOc1 [V1]	12	-84	0	Inf	
L Middle Occipital Gyrus	19	-24	-84	18	Inf	
R Lingual Gyrus	Area hOc3v [V3v]	14	-78	-6	Inf	
R Superior Parietal Lobule	Area 7A (SPL)	22	-60	70	Inf	
L Lingual Gyrus	Area hOc3v [V3v]	-16	-80	-8	Inf	
R Cuneus	Area hOc1 [V1]	14	-92	8	Inf	
L Occipital Pole	18	-8	-98	8	Inf	
Cerebellar Vermis	Lobules VI-VII (Verm)	0	-70	-32	Inf	
L Cerebellum Exterior		-8	-68	-46	5.57	
L Inferior Occipital Gyrus	18	-32	-92	-4	4.97	
L Middle Occipital Gyrus	19	-42	-64	2	Inf	498
R Superior Frontal Gyrus	6	24	0	56	Inf	1222
R Precentral Gyrus	6	24	-14	74	Inf	
R Precentral Gyrus		28	-22	56	7.51	
R Precentral Gyrus		28	-22	64	7.36	
L Superior Frontal Gyrus	6	-24	-2	56	Inf	1037
L Precentral Gyrus		-28	-24	62	5.86	
L Precentral Gyrus		-26	-22	56	5.60	
L Cerebelum (IX)	Lobule IX (Hem)	-14	-48	-50	Inf	647
L Cerebelum (VIII)	Lobule VIIIb (Hem)	-28	-40	-50	Inf	
L Cerebelum (VI)	Lobule VI (Hem)	-30	-36	-34	Inf	
L Cerebelum (Crus 1)	Lobule VI (Hem)	-38	-42	-36	7.53	
L Cerebelum (X)	Lobule V (Hem)	-26	-32	-40	7.19	
L Cerebelum (VI)	Lobule VI (Hem)	-28	-42	-30	7.17	
L Cerebelum (VIII)	Lobule VIIIb (Hem)	-18	-38	-54	6.16	
L Cerebelum (VIII)	Lobule VIIIb (Hem)	-24	-50	-56	6.03	
R Cerebelum (IX)	Lobule IX (Hem)	16	-50	-48	7.57	164
R Cerebelum (VIII)	Lobule VIIIb (Hem)	28	-42	-50	6.32	
R Cerebelum (VIII)	Lobule VIIIb (Hem)	18	-38	-52	5.58	

are suitable for controlling fast movement because the corresponding inertia of the forearm and hand is rather small. On the other hand, proximal muscles have a large body inertia, which is suitable for controlling slow movements [29]. Therefore, our results show that these different muscular systems were reasonably utilized for each condition according to participants' force feeling information in the driving task, as a kind of visuo-motor control tool, rather than a simple power exertion. In contrast, in the context of visuo-motor control, when we exert an action, we predict sensory feedback and modify the motor signals based on the prediction error (e.g. [30], [31]). Likewise, the vehicle response results in less prediction error to steering operation based on driving intention; thus, a driver can maintain motivation without stress, which eventually leads to positive emotions. Moreover, drivers might make predictions based on an internal model [31] acquired from their past experience driving vehicles. In this case, a steering wheel's viscoelasticity can be a control factor for drivers to adapt to the prediction error between the vehicle's reaction expected from their internal model of a vehicle, such as a small car, a large car, and a sporty car, depending on their experiences, as well as age and gender. In recent years, a model-based approach has gained importance for efficient and high-quality product development (e.g. [32]), and for future model-based development, accumulating knowledge on the brain mechanism for the input-output relationship associated with driving will be useful.

In this study, despite using a simplified relationship between steering angles and reaction force, we found a fundamental difference in the effects of stiffness and viscosity on driving behavior and brain activity. To extend our findings, in a future study, we will conduct an experiment using complex steering force characteristics (e.g. Takemura et al. [2]) that closely resemble real vehicles. Participants were instructed to steer as if they were actually

TABLE 4. *(Continued.)* Location and volume of active clusters in the viscosity condition. Brain regions significantly activated at the family-wise error (FWE) thresholds with a corrected p < 0.05 at the voxel level.

(c) Gate period

Region	Area	X (mm)	Y (mm)	Z (mm)	Peak Z	Voxels
L Calcarine Gyrus	hOc1 [V1]	-8	-86	-2	Inf	61302
R Lingual Gyrus	hOc2 [V2]	12	-80	-4	Inf	
R Superior Parietal Lobule	7A	22	-60	56	Inf	
R Middle Occipital Gyrus	19	32	-78	18	Inf	
L Middle Occipital Gyrus	19	-22	-86	18	Inf	
L Superior Parietal Lobule	7A	-18	-64	52	Inf	
R Cuneus	hOc1 [V1]	14	-92	8	Inf	
R Middle Temporal Gyrus	hOc5 [V5/MT]	44	-66	2	Inf	
R Cuneus	18	20	-90	14	Inf	
R Fusiform Gyrus	hOc4v [V4(v)]	26	-74	-10	Inf	
L Middle Temporal Gyrus	19	-42	-66	2	Inf	
L Inferior Occipital Gyrus	19	-44	-66	-2	Inf	
R Superior Frontal Gyrus	6	26	-2	56	Inf	
L Superior Frontal Gyrus	6	-24	-2	56	Inf	
L Superior Frontal Gyrus	6	-22	-4	62	Inf	
R Precentral Gyrus		30	-24	58	Inf	
L Thalamus	Thal: Prefrontal	-12	-18	8	Inf	2848
R Thalamus	Thal: Prefrontal	12	-16	10	Inf	
R Thalamus	Thal: Prefrontal	16	-20	14	Inf	
L Putamen		-24	-8	8	7.23	
N/A		-6	-26	-2	6.86	
N/A	Thal: Prefrontal	8	-22	-4	6.68	
N/A		6	-28	-4	6.50	
N/A	Thal: Prefrontal	-8	-18	-4	6.21	
R Pallidum		22	-4	6	6.11	
R Putamen		28	-16	4	5.90	
N/A		-12	2	10	5.59	
R Thalamus		18	-28	-6	5.34	
L Middle Orbital Gyrus	10	-40	56	-6	Inf	788
L IFG (p. Orbitalis)	10	-38	48	-14	Inf	
L IFG (p. Orbitalis)	47	-42	46	-14	Inf	
L Middle Orbital Gyrus	10	-36	52	-12	Inf	
L Middle Frontal Gyrus	10	-32	58	14	7.70	
L Superior Medial Gyrus	10	-8	62	20	6.87	
L Middle Frontal Gyrus	10	-36	58	2	6.57	
L Superior Frontal Gyrus	Fp1	-18	62	14	5.60	
L Superior Medial Gyrus	10	-4	58	30	5.58	
R Superior Medial Gyrus	Fp2	2	56	4	5.05	
L Superior Medial Gyrus	10	-6	58	6	5.02	
L Insula Lobe	13	-30	16	10	Inf	124
R Middle Frontal Gyrus	10	44	50	14	7.42	778
R Middle Frontal Gyrus	9	38	40	26	6.91	
R Middle Frontal Gyrus	10	44	54	0	6.83	
R Middle Orbital Gyrus	10	42	52	-12	6.61	
R Middle Frontal Gyrus	10	38	42	14	6.48	
R Middle Frontal Gyrus		34	52	28	5.91	
R Middle Orbital Gyrus	Fo3	26	38	-14	5.85	
R Middle Frontal Gyrus	9	38	36	36	5.70	
R IFG (p. Orbitalis)	Fo3	30	34	-16	5.31	
R IFG (p. Orbitalis)	Fo3	26	32	-16	5.24	
L Superior Medial Gyrus	8	-10	44	46	6.40	77
R Superior Frontal Gyrus	8	22	48	42	5.77	20
L Middle Frontal Gyrus	9	-40	34	34	5.78	88
L Middle Frontal Gyrus	9	-46	36	28	5.47	
R IFG (p. Orbitalis)	47	32	28	-18	5.61	10
R IFG (p. Orbitalis)	47	42	24	-18	4.56	
R Superior Frontal Gyrus	Fp1	30	62	6	5.57	11
R Superior Frontal Gyrus	Fp1	26	62	8	5.21	
L IFG (p. Orbitalis)	Fo3	-32	22	-20	5.51	16
L IFG (p. Orbitalis)	Fo3	-34	26	-20	5.48	
L IFG (p. Orbitalis)	47	-34	30	-18	4.88	
R MCC		0	-12	30	5.32	39
L Superior Frontal Gyrus	9	-16	54	36	5.18	10
R Superior Medial Gyrus	9	8	60	28	5.04	36
R Middle Frontal Gyrus		20	60	26	4.90	
L Middle Orbital Gyrus	Fo3	-22	40	-16	4.92	2
L Cerebelum (Crus 2)		-36	-70	-46	4.85	5
R IFG (p. Orbitalis)	47	46	22	-16	4.78	2
R Insula Lobe	Fo3	34	22	-20	4.59	1
Left Posterior Cingulate Gyrus		0	-30	28	4.59	3
L Superior Frontal Gyrus	8	16	38	50	4.58	1
R Superior Medial Gyrus	9	8	56	34	4.52	1

TABLE 5. Location and volume of active clusters. Stiffness condition S3 > S1 at cluster 1.

Region	Area	X (mm)	Y (mm)	Z (mm)	Peak Z	Voxels
L Postcentral Gyrus	1	-46	-24	62	7.43	826
L Precentral Gyrus		-38	-20	64	6.44	
L Postcentral Gyrus	3b	-50	-16	42	5.81	
L Precentral Gyrus		-26	-22	76	5.69	
L Postcentral Gyrus	1	-44	-36	64	5.56	
L Precentral Gyrus		-30	-22	74	5.41	
L Superior Parietal Lobule	7PC	-38	-48	62	5.22	
L Postcentral Gyrus	1	-40	-42	66	5.10	
L Precentral Gyrus		-18	-18	78	4.88	
L Postcentral Gyrus		-52	-12	52	4.87	

Brain regions significantly activated at the family-wise error (FWE) thresholds with a corrected p < 0.05 at the voxel level.

TABLE 6. Location and volume of active clusters. Viscosity condition V3 > V1.

Region	Area	X (mm)	Y (mm)	Z (mm)	Peak Z	Voxels
L Precentral Gyrus		-26	-18	58	5.97	220
L Precentral Gyrus		-24	-14	70	5.68	
L Postcentral Gyrus		-20	-34	76	5.59	120
L Postcentral Gyrus	4a	-32	-32	68	5.25	
L Postcentral Gyrus	2	-24	-40	60	4.84	
R Postcentral Gyrus		28	-28	60	5.49	102
R Postcentral Gyrus		22	-63	52	4.76	

Brain regions significantly activated at the family-wise error (FWE) thresholds with a corrected p < 0.05 at the voxel level and false discovery rate (FDR) with a corrected p < 0.05 at the cluster level.

driving; however, they were not given detailed information on the vehicle, such as whether it was large or small. However, the kind of vehicle they intend to drive might affect steering feelings. To clarify the effects of steering force characteristics on the steering feeling, it will be necessary to define the characteristics of the target vehicle and to use a corresponding vehicle model.

C. SUBJECTIVE PERCEPTIONS

Regarding the results of VAS4 shown in Fig. 10, in the stiffness condition, S2 was rated significantly positive for all VAS4 evaluation words, as predicted by our preliminary pilot study, which can be interpreted as the moderate reaction force being important for positive steering feeling in comparison with S1 and S3. In contrast, regarding the viscous condition, self-efficacy tended to be significantly higher in V2 than in V3. Since V2 was determined as a characteristic with moderate viscosity, it might mean that excessive viscosity might hinder the desired steering. In addition, from the results of principal component analysis (PCA), participants' evaluation followed a single axis reflecting positive-negative feeling.

As for VAS7 after six trials, anxiety was rated significantly higher in S1 than in S2 in the stiffness condition, as shown in Fig. 11(a). This suggests that participants felt anxiety if they experienced no reaction force. In addition, self-efficacy, pleasantness, and excitement were rated significantly higher in S2 than in S1 and S3. This tendency that ratings for positive evaluation words increased in S2 was consistent with the results of VAS4, suggesting that moderate stiffness is related to positive feelings. As for VAS7, in the viscosity condition,

there was no significant difference among the three levels as shown in Fig. 11(b). In the PCA results shown in Fig. 11(c), the first principal component can be interpreted as a positive feeling and the second as unpleasant, with the cumulative contribution rate of the first and second principal components being around 75%. Therefore, these results suggested that the evaluation on a positive-negative feeling was dominant both in VAS4 and VAS7.

Note that the task performance scores presented at the end of each trial resulted in a bias to the steering feeling. Nevertheless, at least the negative-positive feeling varied by changing the viscoelastic characteristics of the reaction force even in the measurement environment using MRI. In addition, the significant change in anxiety rating in VAS7 by different stiffness coefficients may reflect that participants performed the driving task with a mindset to drive a vehicle even in this simple driving simulation.

D. LIMITATIONS

Our experimental settings markedly differed from real-life driving conditions; for instance, participants' postures were supine and the driving task required no acceleration input. To generalize our results to actual driving, we should consider implementing the following improvements in future studies: (1) establishing a method to verify the findings obtained by fMRI in a vehicular driving environment mimicking the real world; (2) improving the driving task to enhance participants' driving pleasure, possibly by using steering reaction force characteristics such that participants may feel the steering reaction force changing linearly with their steering operation (e.g. [2]) and by adopting a challenging driving course. Furthermore, subjective evaluations in this experiment were influenced by the performance score presented after each trial as well as the driving feeling during the trial, because the subjective evaluation was performed after presentation of the performance score at the end of each trial. Therefore, it is difficult to extract brain activity purely related to the driving feeling, and in future work, the experimental design needs to be improved so that participants can perform a subjective evaluation purely reflecting their feelings while performing the driving task; and (3) examining the effects of individual differences in driving ability, such as skills and experience. Moreover, although this experiment targeted only young men to obtain reliable results within a homogeneous subject group, it is necessary to expand the scope of research because of the clear differences in driving behavior and emotional/affect states caused by age and gender [33]–[35].

Considering these issues will lead to a better understanding of the neural mechanisms related to driving pleasure.

V. CONCLUSION

The present study is the first to perform fMRI measurements of brain activity during steering operations in a simulated driving task with variable steering reaction forces. By changing the viscoelastic characteristics of the steering reaction force, we found that the rotational stiffness of the steering wheel mainly affected the distal muscles, whereas the rotational viscosity affected driving control mediated by the proximal muscles. It is possible that these novel and basic findings could provide a neuroscientific method for optimizing steering characteristics based on brain activity.

APPENDIX

See Table 3–6.

REFERENCES

[1] A. W. Burton, "Innovation drivers for electric power-assisted steering," *IEEE Control Syst.*, vol. 23, no. 6, pp. 30–39, Dec. 2003, doi: 10.1109/MCS.2003.1251179.

[2] K. Takemura, N. Yamada, A. Kishi, K. Nishikawa, T. Nouzawa, C. Li, Y. Kurita, and T. Tsuji, "A subjective force perception model of humans and its application to a steering operation system of a vehicle," in *Proc. IEEE Int. Conf. Syst., Man, Cybern.*, Oct. 2013, pp. 3675–3680, doi: 10.1109/SMC.2013.626.

[3] J. Dang, H. Chen, B. Gao, Q. Li, M. Li, T. Watanabe, R. Hayama, L. Lou, and S. Nakano, "Optimal design of on-center steering force characteristic based on correlations between subjective and objective evaluations," *SAE Int. J. Passenger Cars—Mech. Syst.*, vol. 7, no. 3, pp. 992–1001, Apr. 2014, doi: 10.4271/2014-01-0137.

[4] A. J. Pick and D. J. Cole, "Neuromuscular dynamics in the driver–vehicle system," *Vehicle Syst. Dyn.*, vol. 44, no. sup1, pp. 624–631, Jan. 2006, doi: 10.1080/00423110600882704.

[5] C. Dijksterhuis, K. A. Brookhuis, and D. De Waard, "Effects of steering demand on lane keeping behaviour, self-reports, and physiology. A simulator study," *Accident Anal. Prevention*, vol. 43, no. 3, pp. 1074–1081, May 2011, doi: 10.1016/j.aap.2010.12.014.

[6] J. Navarro, E. Reynaud, and F. Osiurak, "Neuroergonomics of car driving: A critical meta-analysis of neuroimaging data on the human brain behind the wheel," *Neurosci. Biobehavioral Rev.*, vol. 95, pp. 464–479, Dec. 2018, doi: 10.1016/j.neubiorev.2018.10.016.

[7] P. A. Hancock and J. L. Szalma, "The future of neuroergonomics," *Theor. Issues Ergonom. Sci.*, vol. 4, nos. 1–2, pp. 238–249, Jan. 2003, doi: 10.1080/1463922021000020927.

[8] R. Parasuraman, "Neuroergonomics: Research and practice," *Theor. Issues Ergonom. Sci.*, vol. 4, nos. 1–2, pp. 5–20, Jan. 2003, doi: 10.1080/14639220210199753.

[9] V. D. Calhoun and G. D. Pearlson, "A selective review of simulated driving studies: Combining naturalistic and hybrid paradigms, analysis approaches, and future directions," *NeuroImage*, vol. 59, no. 1, pp. 25–35, Jan. 2012, doi: 10.1016/j.neuroimage.2011.06.037.

[10] K. Kan, T. A. Schweizer, F. Tam, and S. J. Graham, "Methodology for functional MRI of simulated driving," *Med. Phys.*, vol. 40, no. 1, Jan. 2013, Art. no. 012301, doi: 10.1118/1.4769107.

[11] Y. Okamoto, T. Sasaoka, T. Yoshida, K. Takemura, Z. Soh, T. Nouzawa, S. Yamawaki, and T. Tsuji, "Development of fMRI-compatible steering reaction force generation unit," *IEEE/ASME Trans. Mechatronics*, vol. 24, no. 2, pp. 549–560, Apr. 2019, doi: 10.1109/TMECH.2019.2895456.

[12] R. C. Oldfield, "The assessment and analysis of handedness: The Edinburgh inventory," *Neuropsychologia*, vol. 9, no. 1, pp. 97–113, 1971, doi: 10.1016/0028-3932(71)90067-4.

[13] J. A. Russell, "A circumplex model of affect.," *J. Personality Social Psychol.*, vol. 39, no. 6, pp. 1161–1178, 1980, doi: 10.1037/h0077714.

[14] *Wellcome Department of Cognitive Neurology*. Accessed: Mar. 23, 2016. [Online]. Available: www.fil.ion.ucl.ac.uk/spm

[15] L. Griffanti, G. Salimi-Khorshidi, C. F. Beckmann, E. J. Auerbach, G. Douaud, C. E. Sexton, E. Zsoldos, K. P. Ebmeier, N. Filippini, C. E. Mackay, S. Moeller, J. Xu, E. Yacoub, G. Baselli, K. Ugurbil, K. L. Miller, and S. M. Smith, "ICA-based artefact removal and accelerated fMRI acquisition for improved resting state network imaging," *NeuroImage*, vol. 95, pp. 232–247, Jul. 2014, doi: 10.1016/j.neuroimage.2014.03.034.

[16] L. Griffanti, G. Douaud, J. Bijsterbosch, S. Evangelisti, F. Alfaro-Almagro, M. F. Glasser, E. P. Duff, S. Fitzgibbon, R. Westphal, D. Carone, C. F. Beckmann, and S. M. Smith, "Hand classification of fMRI ICA noise components," *NeuroImage*, vol. 154, pp. 188–205, Jul. 2017, doi: 10.1016/j.neuroimage.2016.12.036.

[17] S. B. Eickhoff, K. E. Stephan, H. Mohlberg, C. Grefkes, G. R. Fink, K. Amunts, and K. Zilles, "A new SPM toolbox for combining probabilistic cytoarchitectonic maps and functional imaging data," *NeuroImage*, vol. 25, no. 4, pp. 1325–1335, May 2005, doi: 10.1016/j.neuroimage.2004.12.034.

[18] S. B. Eickhoff, S. Heim, K. Zilles, and K. Amunts, "Testing anatomically specified hypotheses in functional imaging using cytoarchitectonic maps," *NeuroImage*, vol. 32, no. 2, pp. 570–582, Aug. 2006, doi: 10.1016/j.neuroimage.2006.04.204.

[19] S. B. Eickhoff, T. Paus, S. Caspers, M.-H. Grosbras, A. C. Evans, K. Zilles, and K. Amunts, "Assignment of functional activations to probabilistic cytoarchitectonic areas revisited," *NeuroImage*, vol. 36, no. 3, pp. 511–521, Jul. 2007, doi: 10.1016/j.neuroimage.2007.03.060.

[20] J. L. Lancaster, M. G. Woldorff, L. M. Parsons, M. Liotti, C. S. Freitas, L. Rainey, P. V. Kochunov, D. Nickerson, S. A. Mikiten, and P. T. Fox, "Automated talairach atlas labels for functional brain mapping," *Hum. Brain Mapping*, vol. 10, no. 3, pp. 120–131, Jun. 2000, doi: 10.1002/1097-0193(200007)10:3<120::AID-HBM30>3.0.CO;2-8.

[21] J. L. Lancaster, L. H. Rainey, J. L. Summerlin, C. S. Freitas, P. T. Fox, A. C. Evans, A. W. Toga, and J. C. Mazziotta, "Automated labeling of the human brain: A preliminary report on the development and evaluation of a forward-transform method," *Hum. Brain Mapping*, vol. 5, no. 4, pp. 238–242, 1997, doi: 10.1002/(SICI)1097-0193(1997)5:4<238::AID-HBM6>3.0.CO;2-4.

[22] J. Germann, M. M. Chakravarty, D. L. Collins, and M. Petrides, "Tight coupling between morphological features of the central sulcus and somatomotor body representations: A combined anatomical and functional MRI study," *Cerebral Cortex*, vol. 30, no. 3, pp. 1843–1854, Mar. 2020, doi: 10.1093/cercor/bhz208.

[23] J. G. Colebatch, M. P. Deiber, R. E. Passingham, K. J. Friston, and R. S. Frackowiak, "Regional cerebral blood flow during voluntary arm and hand movements in human subjects," *J. Neurophysiology*, vol. 65, no. 6, pp. 1392–1401, Jun. 1991, doi: 10.1152/jn.1991.65.6.1392.

[24] D. E. Vaillancourt, K. R. Thulborn, and D. M. Corcos, "Neural basis for the processes that underlie visually guided and internally guided force control in humans," *J. Neurophysiology*, vol. 90, no. 5, pp. 3330–3340, Nov. 2003, doi: 10.1152/jn.00394.2003.

[25] T. A. Yousry, U. D. Schmid, H. Alkadhi, D. Schmidt, A. Peraud, A. Buettner, and P. Winkler, "Localization of the motor hand area to a knob on the precentral gyrus. A new landmark," *Brain*, vol. 120, no. 1, pp. 141–157, Jan. 1997, doi: 10.1093/brain/120.1.141.

[26] S. T. Grafton, R. P. Woods, and J. C. Mazziotta, "Within-arm somatotopy in human motor areas determined by positron emission tomography imaging of cerebral blood flow," *Exp. Brain Res.*, vol. 95, no. 1, pp. 172–176, Jul. 1993, doi: 10.1007/bf00229666.

[27] H. J. Freund, "Clinical aspects of premotor function," *Behav Brain Res*, vol. 18, no. 2, pp. 187–191, Nov.-Dec. 1985, doi: 10.1016/0166-4328(85)90074-9.

[28] *Chassis Handbook*, Springer, Cham, Switzerland, 2011.

[29] R. F. Chandler, C. E. Clauser, J. T. McConville, H. M. Reynolds, and J. W. Young, "Investigation of inertial properties of the human body," *Nat. Highway Traffic Saf. Admin.*, vol. no., pp. 1–169, Mar. 1975.

[30] T. Tsuji and Y. Tanaka, "Bio-mimetic impedance control of robotic manipulator for dynamic contact tasks," *Robot. Auto. Syst.*, vol. 56, no. 4, pp. 306–316, Apr. 2008, doi: 10.1016/j.robot.2007.09.001.

[31] D. M. Wolpert and Z. Ghahramani, "Computational principles of movement neuroscience," *Nature Neurosci.*, vol. 3, no. S11, pp. 1212–1217, Nov. 2000, doi: 10.1038/81497.

[32] H. Kimpara, K. C. Mbanisi, J. Fu, Z. Li, D. Prokhorov, and M. A. Gennert, "Human model-based active driving system in vehicular dynamic simulation," *IEEE Trans. Intell. Transp. Syst.*, vol. 21, no. 5, pp. 1903–1914, May 2020, doi: 10.1109/TITS.2019.2906294.

[33] N. Rhodes and K. Pivik, "Age and gender differences in risky driving: The roles of positive affect and risk perception," *Accident Anal. Prevention*, vol. 43, no. 3, pp. 923–931, May 2011, doi: 10.1016/j.aap.2010.11.015.

[34] C. Turner and R. McClure, "Age and gender differences in risk-taking behaviour as an explanation for high incidence of motor vehicle crashes as a driver in young males," *Injury Control Saf. Promotion*, vol. 10, no. 3, pp. 123–130, Sep. 2003, doi: 10.1076/icsp.10.3.123.14560.

[35] E. C. Andrews and S. J. Westerman, "Age differences in simulated driving performance: Compensatory processes," *Accident Anal. Prevention*, vol. 45, pp. 660–668, Mar. 2012, doi: 10.1016/j.aap.2011.09.047.

YOSHIHISA OKAMOTO (Member, IEEE) received the B.E. and M.E. degrees in precision engineering from Osaka University, Japan, in 1982 and 1985, respectively. He is currently pursuing the Ph.D. degree in mechanical engineering with Hiroshima University, Hiroshima, Japan. He has been with Mazda Motor Corporation since 1985. His research interest includes the brain function during car driving.

TAKAFUMI SASAOKA received the Ph.D. degree in informatics from Kyoto University, in 2003. Since 2018, he has been an Associate Professor with the Center for Brain, Mind and KANSEI Sciences Research, Hiroshima University. He has been a Research Leader of the Center of Innovation, KANSEI Research Project, since 2019. His research interests include cognitive psychology and neuroscience.

NORIHIRO SADATO received the M.D. degree from the Faculty of Medicine, Kyoto University, in 1983, and the Ph.D. degree from the Faculty of Medicine (Nuclear Medicine), Kyoto University, in 1994. He has been a Professor with the National Institute for Physiological Sciences, Japan, since 1999. After trained as a diagnostic radiologist, he entered into the functional neuroimaging field in 1990. He is interested in understanding the mechanisms of plastic change in the human brain accompanied by learning, sensory deprivation, and development explored by functional magnetic resonance imaging (MRI). He currently focuses on the development of social cognition and its correlates. He has been the Chair of the Ethics Committee of The Japan Neuroscience Society, since 2008.

MASAKI FUKUNAGA received the B.S., M.S., and Ph.D. degrees in acupuncture and moxibustion from the Meiji University of Oriental Medicine, Kyoto, Japan, in 2000. From 2003 to 2010, he was a Research Fellow with the Advanced MRI Section, Laboratory of Functional and Molecular Imaging, National Institute of Neurological Disorders and Stroke, National Institutes of Health, Bethesda, MD, USA. From 2010 to 2014, he was an Assistant Professor with the Biofunctional Imaging, Immunology Frontier Research Center, Osaka University, Osaka, Japan. Since 2014, he has been an Associate Professor with the Division of Cerebral Integration, National Institute for Physiological Sciences, Okazaki, Japan. He has authored more than 100 peer-reviewed articles and book chapters in the field of MRI. His current research interests include technical development and neuroscience application of ultrahigh field MRI.
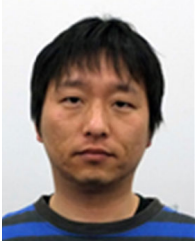
TETSUYA YAMAMOTO (Member, IEEE) received the B.S. degree in integrated human studies, and the M.S. and Ph.D. degrees in human and environmental studies from Kyoto University, Kyoto, Japan, in 2003, 2005, and 2010, respectively. He was a Postdoctoral Fellow with the Graduate School of Medicine, Kyoto University, from 2008 to 2010, the Kokoro Research Center, Kyoto University, from 2010 to 2013, the Department of Electrical Engineering, Graduate School of Engineering, Kyoto University, from 2013 to 2016, and the National Institute for Physiological Sciences, Okazaki, Japan, from 2016 to 2019. Since 2019, he has been a Project Assistant Professor with the National Institute for Physiological Sciences, Okazaki. His research interests include human brain functional imaging on depth and motion perception, visual topography, and eye movement using functional magnetic resonance imaging (fMRI), geometric distortion corrections and noise reduction of fMRI data, and the development of ultra-low field MRI. His awards and honors include the Research Fellowship for the Young Scientists of the Japan Society for the Promotion of Science from 2005 to 2008, the IEEE Computational Intelligence Society Japan Chapter Young Researcher Award in 2011, the Distinguished Service Award of the Japan Society of Japan in 2018, and the Young Scientist Award of the Japan Human Brain Mapping Society in 2018.
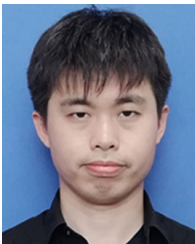
ZU SOH (Member, IEEE) received the B.E., M.E., and D.Eng. degrees in electrical and electronic engineering from Hiroshima University, Hiroshima, Japan, in 2006, 2008, and 2010, respectively. He was a Research Fellow with the Japan Society for the Promotion of Science from 2008 to 2013. He has been an Assistant Professor with the Department of System Cybernetics, Hiroshima University, since 2013. His current research interests include biological signal analysis, artificial life, and biological modeling.

TAKAHIDE NOUZAWA received the B.E. degree in chemical engineering, and the M.E. and D.Eng. degrees in transport phenomena engineering from Hiroshima University, Hiroshima, Japan, in 1978, 1980, and 1994, respectively. He is currently a Professor (Special Appointment) with the Office of Research and Academia-Government-Community Collaboration, Hiroshima University. From 2010 to 2020, he was a General Manager and a Technical Fellow with the Mazda Technical Research Center. From 2014 to 2019, he was also a Project Leader of the Center of Innovation national project at the Center of Kansei Innovation, Hiroshima University. His current research is interested in human–machine interface, Kansei brain science, and aerodynamics of vehicle.

SHIGETO YAMAWAKI received the degree from the School of Medicine, Hiroshima University, in 1979. He has been a Professor and the Chairman of the Department of Psychiatry and Neurosciences, Hiroshima University, since 1990. He served as the President of International College of Neuropsychopharmacology, from 2014 to 2016. He is currently a Professor Emeritus with Hiroshima University.

TOSHIO TSUJI (Member, IEEE) received the B.E. degree in industrial engineering, and the M.E. and D.Eng. degrees in systems engineering from Hiroshima University, Hiroshima, Japan, in 1982, 1985, and 1989, respectively. He is currently a Full Professor with the Graduate School of Advanced Science and Engineering, Hiroshima University. His research interests range from engineering to human science, with focuses on cybernetics, medical electronics, computational neural sciences, and particularly biological Kansei modeling. He has received 42 academic awards, including the IEEE 2003 King-Sun Fu Memorial Best Transactions Paper Award.

• • •